



Effects of nano eggshell powder as a sustainable bio-filler on the physical, rheological, and microstructure properties of bitumen

Alattafi Hadi Zghair Chfat^a, Haryati Yaacob^{a,*}, Nurul Hidayah Mohd Kamaruddin^b, Zaid Hazim Al-Saffar^c, Ramadhansyah Putra Jaya^d

^a Faculty of Civil Engineering, Department of Geotechnics and Transportation, Universiti Teknologi Malaysia, 81310, UTM, Johor Bahru, Malaysia

^b Faculty of Civil Engineering and Built Environment, Universiti Tun Hussein Onn Malaysia, Johor Bahru, Malaysia

^c Building and Construction Engineering Department, Engineering Technical College of Mosul, Northern Technical University, Mosul, 41002, Iraq

^d Faculty of Civil Engineering Technology, Universiti Malaysia Pahang Al-Sultan Abdullah, 26300, Kuantan, Pahang, Malaysia

ARTICLE INFO

Keywords:

Nano eggshell powder
Bitumen
Physical properties
Rheological properties
Microstructure properties

ABSTRACT

Improving bitumen properties to withstand traffic loads and environmental conditions is essential for prolonging pavement life. Given that nanomaterials stand as potential candidates to fulfil these requirements, this study focused on the potential use of nano eggshell powder (NESP) as a sustainable additive in bitumen. NESP was produced using a top-down approach with a ball milling machine. Then, 0% (control), 1%, 3%, 5%, 7%, and 9% NESP by weight of bitumen PEN 60/70 was added. Storage stability and X-Ray Diffraction (XRD) tests were performed to assess the compatibility and dispersion of NESP within the bitumen matrix. Penetration, softening point, ductility, viscosity, and dynamic shear rheometer (DSR) tests were performed to assess the physical and rheological properties of the modified bitumen. Fourier Transform Infrared (FTIR), Atomic Force Microscopy (AFM), contact angle, and thermal analysis (TGA) tests were conducted to analyze the microstructure properties. The results from storage stability tests and XRD patterns suggested that NESP was effectively integrated and evenly dispersed within the bitumen matrix. The incorporation of NESP led to improvement in the hardness and cohesion of the bitumen, as evidenced by reductions in penetration and increase in the softening point. However, higher concentrations of NESP resulted in decreased ductility of the bitumen. The addition of NESP into the bitumen resulted in increased viscosity and improved resistance to aging and rutting. Furthermore, the adhesion and thermal properties of bitumen improved with higher NESP content. Notably, the most effective concentration for enhancing bitumen properties was found to be 9% NESP.

1. Introduction

Bitumen, being a viscoelastic material, is highly influenced by temperature fluctuations. Insufficient physical characteristics, such as stiffness and temperature sensitivity, along with rheological properties (resistance to rutting and fatigue cracking) exacerbate this issue [1,2]. Therefore, modification of the bitumen is necessary to withstand increased traffic loading and temperature changes. The selection of a suitable modifier varies from one country to another, depending on environmental conditions and material availability. Furthermore, the sole consideration for selecting the appropriate modifier should not only be the improvement rate of bitumen performance. Other factors, such as economic considerations and manufacturing technology, should also be taken into account when choosing additive materials [3]. Various types

of bitumen modifiers, including polymers, crumb rubbers, various waste materials, ashes, and fibers, have been utilized to enhance the properties of bitumen, resulting in significant improvements in its performance [4]. However, these modifiers have several drawbacks, including poor high-temperature storage stability and compatibility issues arising from significant differences in density, polarity, molecular weight, and solubility between the polymer and the bitumen [3,5–7]. For example, SBS-modified bitumen is currently the most widely used binder for asphalt pavements, but it has drawbacks, such as inadequate thermal storage stability [8–10]. Research conducted by Zhang et al. [11] highlights a phenomenon where SBS particles tend to aggregate upwards due to their low density during the storage of modified bitumen at high temperatures (typically above 135 °C), leading to a higher concentration of SBS in the upper section and a lower concentration in the

* Corresponding author

E-mail address: haryatiyaacob@utm.my (H. Yaacob).

<https://doi.org/10.1016/j.rineng.2024.102061>

Received 4 February 2024; Received in revised form 11 March 2024; Accepted 25 March 2024

Available online 2 April 2024

2590-1230/© 2024 The Authors. Published by Elsevier B.V. This is an open access article under the CC BY-NC-ND license (<http://creativecommons.org/licenses/by-nc-nd/4.0/>).

lower section of the bitumen. This segregation issue poses significant challenges for construction teams. According to data from the bitumen detection database of the Shandong Academy of Transportation Sciences in China over 11 years [11], approximately 30% of SBS-modified bitumen fails to meet usage specifications or approaches the upper limit of specification requirements. Therefore, improving the properties of these additives materials involves extra costs, making them unsuitable for large-scale use [12,13].

In recent years, nanotechnology has been progressively integrated into bitumen, employing various types of nanomaterials for enhancing bitumen properties [4]. These nanosized particles typically range in size from 1 nm to 100 nm. Nanomaterials possess unique properties, including a large surface area and high dispersion ability, making them effective additives for enhancing and modifying asphalt mixtures [14]. It is also observed that materials, which are inert in their bulk form, exhibit higher reactivity when produced in their nanoscale form [15]. According to FHWA [16], one of the long-term effects of incorporating nanomaterials in pavement research is the development of novel pavement materials with high resistance to traffic and environmental conditions [1]. Past studies have shown that nanomaterials have a significant positive impact on the rheological and mechanical properties of bitumen and asphalt mixtures [17]. Different types of nanomaterials have been used to enhance the properties of bitumen. These nanomaterials encompass nano clay (NC), nano silica (NS), carbon nanofiber (CNF), nano zinc oxide (ZnO), nano titanium (TiO₂), and others. Cadornin et al. [18] reported that nano-TiO₂ improved the rheological behaviour of bitumen, enhancing its resistance to rutting, fatigue, and aging. Shafabakhsh et al. [19] demonstrated that the addition of SiO₂ and TiO₂ nanoparticles to bitumen improved both its rheological behaviour and aging resistance. Ghanoun et al. [20] investigated the impact of nano clay on bitumen modification, revealing that the incorporation of nano clay improved rheological characteristics and resistance to rutting. Mohammed and Abed [21] found that nano-SiO₂ (NS) and nano CaCO₃ (NCC) enhanced the physical and rheological properties of bitumen across low, medium, and high temperatures. However, the majority of common nano additives are manufactured through complex and costly production processes, rendering them impractical for a broad spectrum of road projects [3,22]. Consequently, the challenge lies in utilizing nanomaterials that can be produced inexpensively and in large quantities to enhance bitumen properties. One potential solution is to create nanomaterials from waste materials, thereby mitigating the environmental impact of these wastes and presenting an excellent opportunity to explore their properties through nanotechnology approaches.

The utilization of biomaterial waste in the road construction industry has garnered global attention recently, primarily owing to its renewability and environmental friendliness [23,24]. Moreover, due to the high consumption of bitumen, a non-renewable resource, numerous researchers have endeavoured to identify sustainable and renewable materials as alternatives to petroleum products or to diminish their usage through various methods [25]. Biomaterials derived from animals are commonly produced from organic waste, which, if not properly managed, can be environmentally harmful. The use of these biomaterials in the road construction industry leads to the consumption of significant amounts of hazardous waste [26]. Biomaterial wastes, such as bio-oil and lignin, oyster shells, fish shells, and crayfish shells, have proven to be effective for bitumen modification [27–29]. For example, incorporating bio-oil from rapeseed with lignin can enhance the medium-low temperature performance of bitumen [30]. The stiffness, high-temperature stability, and creep resistance of bitumen can be improved by waste crayfish shell powder [23]. Additionally, oyster shell powder could increase viscosity and improve resistance to rheological deformation of bitumen [29].

Among all types of biomaterial waste, eggshells have garnered significant attention as a low-cost biological waste. Upcycling this material not only contributes to environmental protection but also transforms waste into a valuable resource [25,31,32]. According to the

Environmental Protection Agency, eggshell waste ranks as the fifteenth main cause of environmental pollution [33]. In many countries, the disposal of eggshell waste poses a major concern due to higher land-filling costs and environmental problems. For example, in the US and Europe, egg breaking plants pay approximately USD \$100,000 per year to dispose of eggshells in landfills [34]. Moreover, decomposition of eggshells produces compounds like ammonia, hydrogen sulfide, and amines, releasing high levels of contaminants and odors. Additionally, eggshells can harbor pathogens such as *Escherichia coli* (*E. coli*) and salmonella [35–37]. Globally, it is estimated that approximately 7 million tons of eggshell waste are generated each year [38]. Furthermore, global egg production is expected to increase by approximately 90 million tons by 2030 [39]. In Malaysia, the annual production of chicken eggs amounts to around 642,600 tons, resulting in approximately 70, 686 tons of eggshell waste [40].

The high calcium carbonate content in eggshell waste makes it a valuable material for enhancing the performance of bitumen materials [26]. Limited studies have investigated the use of eggshell as a bitumen modifier and demonstrated its ability to improve bitumen properties [25,26,41]. Wang et al. [25] observed that the addition of eggshell powder enhanced the rutting performance of bitumen, as evidenced by an increase in the $G^*/\sin\delta$ value. The incorporation of eggshell powder not only improves the physical properties of bitumen but also increases its resistance to rutting [26]. In a study by Syammaun et al. [41], the physical and rheological properties of a bitumen binder containing eggshell ash (ESA) were evaluated. The findings indicated that eggshell ash significantly enhanced resistance to high temperatures and improved deformation resistance.

Previous studies showed the incorporation of eggshell powder into bitumen was limited in micro size, and the tests carried out were very limited. Additionally, there was a paucity of research examining performance over the service life under aging conditions and the microstructural behaviour of the modified binder. Understanding these aspects is crucial for evaluating the overall performance of bitumen. Furthermore, due to substantial disparities in density and molecular weight between eggshell powder and bitumen, weak adhesion bonds form between them. This weak adhesion results in several drawbacks in the bitumen, including reduced storage stability at high temperatures, leading to the separation of the eggshell powder from the bitumen during storage, and the loss of all benefits obtained from the modification [5,6,12,42]. Moreover, the large size of eggshell powder particles impedes the free movement of the bitumen mass and diminishes its tensile strength [26]. Therefore, the primary aim of this research is to transform eggshell powder into nanomaterials for the modification of bitumen, with the objective of addressing the aforementioned problems and examining its effect on the physical, rheological, and microstructural properties of bitumen.

2. Materials and method

2.1. Bitumen

The bitumen utilized in this study was PEN 60/70, which is widely used in Malaysia and was obtained from the Kemaman Bitumen Company (KBC). The physical and rheological properties of this bitumen complied with both local and international standards, as demonstrated in Table 1.

2.2. Processing nano eggshell powder

Waste eggshells, obtained from local fast-food establishments, underwent a series of steps for preparation. Initially, they were gathered, cleansed, and immersed in an aqueous NaCl solution for 1 h to eliminate the shell membranes [26]. Afterward, they were dried in a 100 °C oven for 24 h. Following the drying process, an electric mill was employed to grind the eggshells into a powder, which was subsequently sifted

Table 1
Properties of bitumen PEN 60/70.

Properties tests	Results	Requirements [43]	Standard
Penetration at 25 °C (dmm)	62	60–70	ASTM D5/D5M [44]
Softening point (%C)	49.2	49–56	ASTM D36/D36 M [45]
Viscosity at 135 °C (Pa·s)	0.606	<3 Pa·s	ASTM D4402/D4402 M [46]
G*/sinδ (kPa) at 64 °C	2.65	>1 kPa	ASTM D7175 [47]

through a 45 µm sieve. Eggshell powder was converted to nano size by using the top-down method in a ball milling machine (NQM-0.4 Model Plantary Ball Mill) using the trial method (time and rpm) to achieve less than 100 nm in size. The grinding times were 2, 4, 6, and 7 h. For each grinding period, 100 g of material was fed into the ball mill. Fig. 1 shows the process involved. The particle size was examined by a particle size analyzer (PSA) and transmission electron microscopy (TEM).

2.2.1. Particle-size analysis (PSA)

The Brookhaven Particle Size Analyzer (PSA) was used to assess the average particle size of grinded eggshell powder samples over durations of 2, 4, 6, and 7 h. The dynamic light scattering technique, capable of measuring particle sizes within the 0.3 nm to 10 µm range, was utilized for this analysis. To ensure adequate dispersion, the sample underwent a 24-h dilution in distilled water. The testing procedure required only a small sample volume, with concentrations ranging from 0.1 mg/mL to 40% w/v of the sample.

2.2.2. Transmission electron microscopy (TEM)

Transmission Electron Microscopy (TEM) was employed to obtain a higher resolution image and to further analyze the nano size determined by PSA. TEM has the capacity to visualize and analyze samples ranging from 1 µm to 1 nm in size. In this experiment, a limited quantity of particles was suspended in a solvent before undergoing sonication. The sonication process lasted approximately 25 s to ensure the proper dispersion of the particles, after which the sample was allowed to dry. Subsequently, the image of the dried sample was analyzed.

2.3. Bitumen modification process

NESP-modified bitumen was prepared at various concentrations: 0.0% (as control bitumen), 1.0%, 3.0%, 5.0%, 7.0%, and 9.0% of NESP by weight of bitumen. These concentrations were selected to evaluate the effect of NESP content on bitumen sensitivity and determine the optimal NESP content. The blending process took place using a high-shear mixer at 3000 rpm for 40 min at a temperature of 160 ± 10 °C. These parameters were chosen based on prior studies involving the mixing of nanomaterials [14,48,49]. The mixing speed of 3000 rpm was selected to prevent agglomeration of nanomaterials with speeds below 3000 rpm [49]. The temperature of 160 °C was selected to prevent bitumen aging at high temperatures, and a mixing time of 40 min was chosen to ensure proper blending of the NESP [1]. To study the effects of NESP on the physical, rheological, and microstructural properties of bitumen, various tests were conducted as shown in Table 2.

Table 2
Tests and number of samples conducted in this study.

No.	Test	No of samples	Total no of samples for (0%,1%,3%,5%,7%, and 9%NESP)
1	Storage stability	3	18
2	Penetration	3	18
3	Softening point	3	18
4	Ductility	3	18
5	Viscosity	3	18
6	DSR Unaged	3	18
	Aged (RTFO)	3	18
7	XRD	1	6
8	FTIR	1	6
9	AFM	1	4
10	Contact angle	3	18
11	TGA	1	6
Total number of samples			166

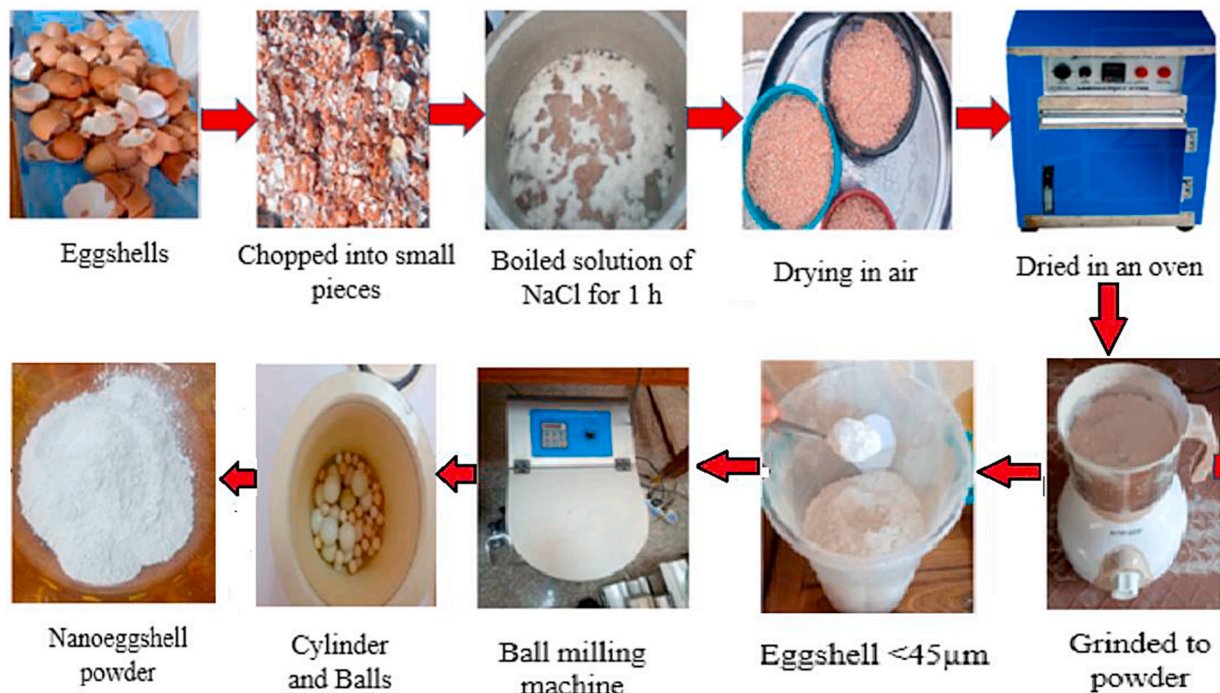


Fig. 1. Nano eggshell powder preparation method.

2.4. Bitumen properties tests

2.4.1. Storage stability test

This test was carried out in accordance with ASTM-D5976 [50]. Storage stability refers to the tendency of modified bitumen compounds to separate during storage and handling in the field and provides an indication of the degree of chemical compatibility between two different materials. An aluminium tube (25 mm by 140 mm) was filled with 50 g of the modified bitumen and placed vertically in an oven at 163 °C for 48 h. Afterward, the samples were placed in a freezer at -6.3 °C for 4 h. After removing the sample from the freezer, it was divided into three equal sections. The softening point of the bitumen's top and bottom sections was then determined. The modified bitumen is considered homogeneous and stable during storage at high temperatures if the temperature difference between the softening points of the top and bottom portions does not exceed 2.2 °C.

2.4.2. X-Ray diffraction test (XRD) test

X-ray diffraction (XRD) is a technique that employs X-ray radiation to determine the crystal structure of an unknown material. The X-rays are diffracted according to the position, arrangement, and size of the crystal constituents. It also provides an indication of the degree of compatibility between bitumen and a modifier. In this test, the (Rigaku SmartLab) device, was used to analyze a bitumen sample. In this study, XRD patterns were used to assess the degree of dispersion of NESP within the bitumen matrix.

2.4.3. Penetration test

The penetration test was employed to assess the hardness of the bitumen, in accordance with the ASTM D5/D5M [44]. A lower penetration value indicates higher bitumen hardness. Prior to the test, the bitumen was heated and poured into a penetration cup. Following this, the sample underwent a 1-h immersion in a water bath at 25 °C. After the cooling process, the penetration test was then conducted using the equipment, applying a total load of 100 g for 5 s at 25 °C.

2.4.4. Softening point test

The softening point test is used to determine the temperature at which a phase change occurs and as a gauge the temperature susceptibility of the bitumen. This test was carried out in accordance with ASTM D36/D36 M [45]. The procedure involved heating the bitumen, pouring it into two rings, and allowing it to cool for 30 min. Following this, the two rings and two ball centring guides were positioned on the ring holder within a water bath. Subsequently, steel balls weighing 3.5 g each were placed on each bitumen sample and heated. The recorded temperature at which the bitumen contacted the base plate was noted, and the average temperature of the two samples was then computed.

2.4.5. Viscosity test

This test was conducted in accordance with ASTM D4402/D4402 M [46]. Viscosity was used to determine the flow resistance and internal friction of the bitumen. Viscosity measurements were taken at two temperatures: 135 °C and 165 °C. Rotational viscosity was determined using a Brookfield viscometer and a thermostat system. A cylindrical spindle with the size number LV-3 (63) was immersed in the bitumen at a constant temperature, and the torque required to maintain the spindle's constant rotational speed of 20 rpm was calculated. This torque is related to the viscosity of the binder. Mixing and compaction temperatures can be calculated from the results of this test.

2.4.6. Penetration index (PI) and penetration–viscosity number (PVN)

The relationship between penetration–softening point and penetration viscosity can be expressed using PI and PVN, as explained in equations (1) and (2), respectively [51]. These indicators were used to assess the bitumen's temperature susceptibility:

$$PI = \frac{1952 - 500 \log P - 20SP}{50 \log P - SP - 120} \quad (1)$$

$$PVN = -1.5 \left(\frac{4.258 - 0.7967 \log P - \log V}{0.795 - 0.1858 \log P} \right) \quad (2)$$

where P is penetration value (dmm), SP is softening point value (°C) and V is viscosity (Pa·s).

2.4.7. Ductility test

This test assesses the ductility of bitumen by measuring the elongation before breaking when pulled at a predetermined speed and temperature (5 cm/min at 25 °C). The ductility value can offer an early indication of bitumen behaviour under low-temperature conditions. The test was conducted following the guidelines of ASTM D113 [52].

2.4.8. Rolling thin film oven (RTFO)

The Rolling Thin Film Oven (RTFO) is used to simulate bitumen aging during hot mix bitumen mixing and compaction in the field. The test was conducted according to ASTM-D2872 [53]. About 35 g of bitumen was poured into each RTFO bottle. The bottles were then placed in a rotating carriage in an oven heated to 163 °C. The speed of the rotating carriage was 15 rpm for 85 min with an air flow of 4000 mL/min. The mass loss of the bitumen before and after aging was measured.

2.4.9. Dynamic shear rheometer tests

The DSR test was conducted in accordance with ASTM D7175 [47]. The dynamic shear rheometer (DSR) is employed to characterize the viscoelastic behaviour of bitumen by measuring their complex shear modulus (G^*) and phase angle (δ). The test can be performed at high or low temperatures depending on its intended purpose. In this study, the rutting factor parameter ($G^*/\sin\delta$) for both control and modified bitumen was assessed in the temperature range of 46–82 °C, with an increment of 6 °C, for both unaged and RTFO-conditioned samples. Both aged and unaged samples (modified binder and control) were evaluated against the specific failure criteria outlined in ASTM D7175-15, which are 1.0 kPa for the unaged sample and 2.2 kPa ($|G^*|/\sin\delta$) for the short-term aged sample.

2.4.10. Fourier transform infrared test (FTIR) test

FTIR is a technique for materials analysis. It represents a fingerprint of a sample with absorption peaks that correspond to the frequencies of vibrations between the bonds of the atoms making up the material. This test can give an indication of ageing of bitumen based on functional groups related to the ageing process. A PerkinElmer Frontier FTIR device was used to analyze functional groups for original and NESP-modified bitumen.

2.4.11. Atomic force microscopy (AFM) test

Atomic Force Microscopy (AFM) has the capability to precisely measure material properties at the atomic level while simultaneously offering detailed 3D images. AFM operates in three interaction modes: contact mode, tapping mode, and non-contact mode. The chosen mode depends on the sample's characteristics, including its hardness or stickiness. For the assessment of bitumen morphology, a JPK NanoWizard Atomic Force Microscope was employed, featuring a 300-kHz drive frequency and a 0.5-Hz scan rate at room temperature and atmospheric pressure, utilizing tapping mode. The sample was prepared on the glass slide with dimensions of approximately 1 cm × 1 cm and a thickness of less than 4 mm. Consequently, AFM images of the bitumen matrix microstructure measuring 50 × 50 μm were obtained. The AFM technique is adept at producing topographic images and evaluating bitumen surface roughness at the nanoscale. Two roughness parameters, Ra and Rq, are measured. Ra, the simplest parameter, assesses surface

roughness without considering peaks and valleys. On the other hand, R_q is more sensitive to peaks and valleys.

2.4.12. Contact angle test

The contact angle is the angle created at the point where a liquid meets a solid surface and represents how the liquid spreads over that surface [54]. The contact angle between water droplets and the bitumen surface was used to assess the variations in wettability and the polarity properties resulting from different NESP concentrations. The VCA optima device was used to measure the contact angle.

2.4.13. Thermogravimetric analysis (TGA) test

The TGA is a very efficient technique for thermal analysis, offering valuable information about the decomposition of materials under heating. The weight loss of materials depends on the nature of the material and occurs within a specific range of temperatures [55]. To assess the thermal stability of the bitumen samples, Thermal Gravimetric Analysis (TGA) was performed using a TGA Q500 instrument, following the guidelines of ASTM E1131 [56]. Each sample, weighing 1 mg, was subjected to a nitrogen flow under a heating rate of 10 °C/min within a temperature range of 30–600 °C [57]. The analysis considered the weight loss of the sample relative to the temperature during each experiment. The results of the experiment included the sample's Thermal Gravimetric (TG) and Derivative Thermogravimetric (DTG) curves. The thermal stability of the materials was assessed using the parameters T_{ed} , T_m , and M_f . T_{ed} represents the epitaxial decomposing temperature, T_m denotes the temperature at which the maximal mass loss rate occurs, and M_f signifies the final residue mass ratio [58].

3. Results and discussion

3.1. PSA results

Fig. 2 displays the particle-size distributions of eggshell powder for milling durations of 2, 4, 6, and 7 h. The particle size decreased from 2 h to 6 h of milling time but increased at 7 h. The average particle sizes were 318.1 nm, 172.6 nm, 73.8 nm, and 76.7 nm after milling times of 2, 4, 6, and 7 h, respectively. These findings indicate that a milling time of 6 h resulted in a significant reduction in nanoparticle size (73.8 nm). Furthermore, the increase in nanoparticle size after extending the milling time to 7 h can be attributed to the tendency of particles to agglomerate when they reach the nano size due to van der Waals forces and air influence, as shown in Fig. 3 [59–63]. According to Jeffry et al. [1], prolonged grinding times may not necessarily result in finer sizes even with the same mill power. Wang et al. [61] reported that the ball milling process consists of four stages: welding, compression, smashing, and dynamic equilibrium. During the four stages of the process, the

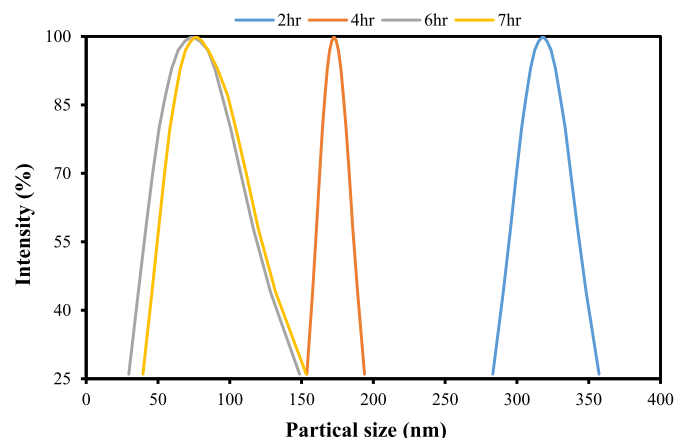


Fig. 2. General size distribution for particles at 2,4,6 and 7 h milling time.



Fig. 3. Eggshell powder after 7 h milling time.

powder experiences varying levels of mechanical stress, leading to the formation of numerous dislocations. This increased density of distortion results in a reduction in particle size as the milling time increases. Nevertheless, the particle size tends to increase beyond the critical time of milling due to the powder reaching the dynamic equilibrium stage. During this stage, particles with higher surface activity and smaller size tend to agglomerate, preventing further reduction in particle size and leading to an increase to some extent. Therefore, the optimal milling duration for producing nano-sized eggshell powder was determined to be 6 h, resulting in an average particle size of 73.8 nm.

3.2. TEM results

High-resolution imaging through Transmission Electron Microscopy (TEM) was utilized to validate the size of nanoparticles generated after 6 h of grinding, as illustrated in Fig. 4. The image was captured at a 100-nm scale. It is evident that the particles displayed irregular shapes, with all dimensions falling within the 1–100 nm range. The particle size varied from 59.91 to 96.03 nm, aligning with the particle size distribution obtained from PSA. These results affirm that the 6-h grinding process was effective in producing nano-sized particles smaller than 100 nm.

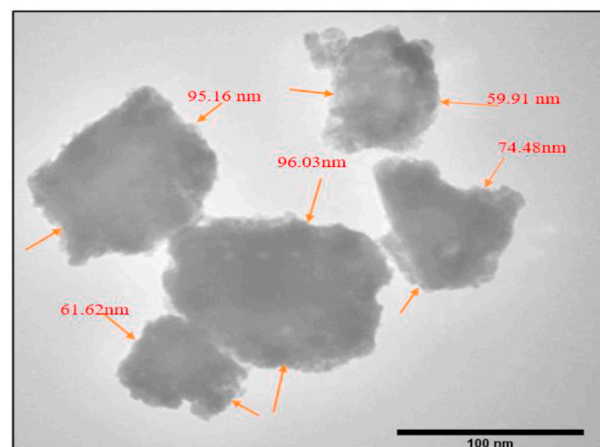


Fig. 4. TEM image of the NESP sample at 100 nm scale.

3.3. Bitumen properties results

3.3.1. Storage stability results

The results of the storage stability test are presented in Table 3. The temperature difference between the upper and lower portions of the modified bitumen meets the specified criterion of being below 2.2 °C ASTM-D5976 [50]. This indicates that the NESP was uniformly dispersed within the bitumen matrix and remained stable and homogeneous despite exposure to high temperatures. The high compatibility between NESP and bitumen suggests that the mixing procedure used to combine these materials was appropriate. This may be attributed to: The extremely large interface area with the bitumen matrix is the most important feature of NESP, resulting in a higher degree of reactivity with the bitumen matrix. Additionally, the nano-size of the eggshell powder makes it easy to disperse within the bitumen matrix. Furthermore, the high calcium carbonate content in NESP, an alkaline material, fosters strong adhesion with bitumen (which is acidic in nature) and prevents phase separation [64].

3.3.2. XRD results

Fig. 5 illustrates the XRD patterns for the control sample and NESP-modified bitumen. Based on Fig. 5, it is evident that the prominent X-ray diffraction (XRD) peak at an angle of $2\theta = 30^\circ$ is associated with the crystalline structures found in bitumen modified with NESP at different proportions. The intensity of the peak at $2\theta = 30^\circ$ progressively increased as the proportion of NESP went from 0% to 9%. An intense XRD peak at $2\theta = 30^\circ$, along with smaller peaks ranging from $2\theta = 35.9^\circ$ to $2\theta = 48.5^\circ$, can be attributed to the crystal structure of CaCO_3 in NESP. The increase in the intensity of peaks observed as the NESP dosage increased from 0 to 9% suggests the stable presence and well-dispersion of NESP within the bitumen matrix [65].

3.3.3. Penetration results

The penetration test is a common method for determining bitumen consistency, with higher penetration values indicating softer and less consistent bitumen. As illustrated in Fig. 6, the penetration of bitumen decreased with increasing nano eggshell powder content. Specifically, the penetration of the NESP-modified bitumen decreased by 4.8%, 8.1%, 10.5%, 14.2%, and 16.0% for 1%, 3%, 5%, 7%, and 9% of NESP, respectively, compared to the 0% (control bitumen). The samples containing 9% NESP demonstrated a higher degree of enhancement. The results of the penetration tests revealed that adding NESP to bitumen could enhance its high-temperature rheological properties by increasing its hardness and consistency. This improvement may be attributed to the high surface area of NESP, which can absorb the oily part of bitumen, thereby increasing the hardness of the bitumen [5,66]. According to Jeffry et al. [1], when the penetration exceeds 30 dmm with proper mixing design and compaction, it exhibits high resistance to cracking; therefore, the values were acceptable because all values exceeded 30 dmm.

3.3.4. Softening point results

The softening point values of the control and NESP-modified bitumen are presented in Fig. 7. The softening point values of NESP-modified bitumen exhibited improvements of 1.8%, 3.7%, 6.5%, 8.9%, and 10.2% for 1%, 3%, 5%, 7%, and 9% NESP, respectively, in

Table 3

Storage stability test of NESP-modified bitumen.

NESP (%)	Difference top and bottom parts (%C)	Requirement < 2.2 °C
1.0	0.5	Pass
3.0	0.5	Pass
5.0	0.5	Pass
7.0	1.0	Pass
9.0	1.0	Pass

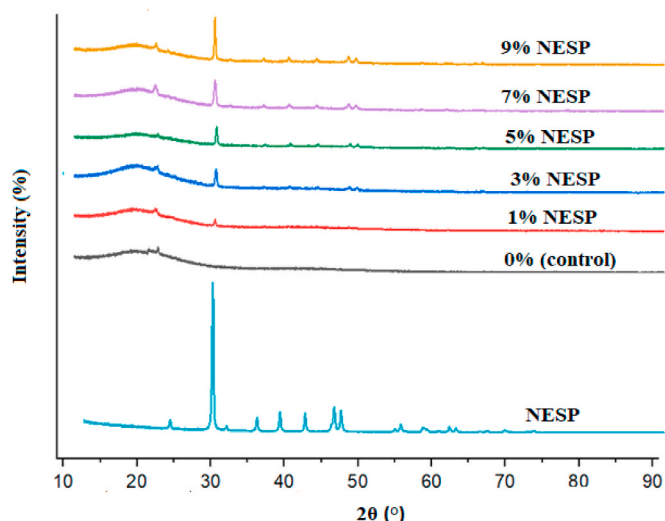


Fig. 5. XRD patterns for control and NESP-modified bitumen.

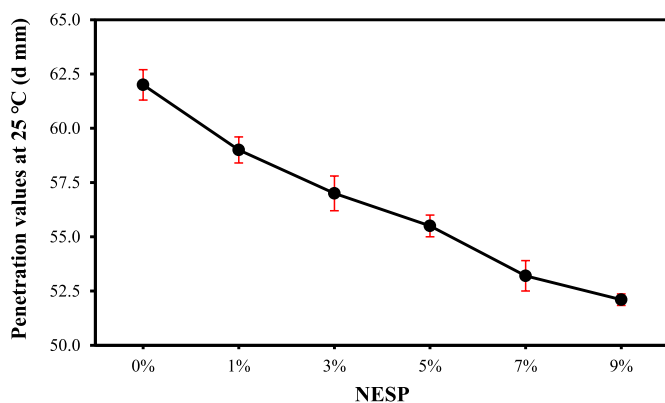


Fig. 6. Penetration results for control and NESP-modified bitumen.

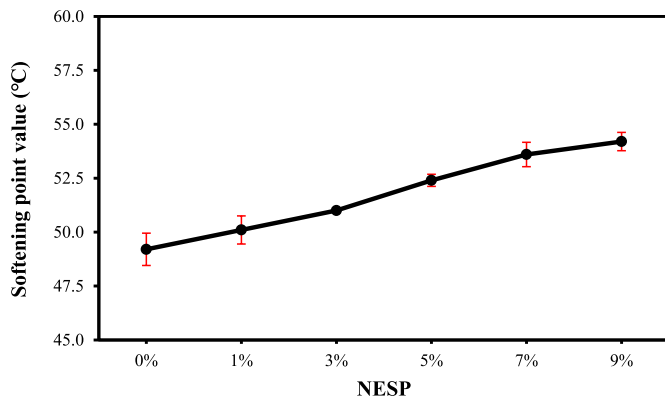


Fig. 7. Softening point values for control and NESP-modified bitumen.

comparison to the control samples. A high softening point signifies the bitumen's ability to endure a specific temperature before transitioning from a solid to a liquid state. This can be attributed to the enhanced cohesion of bitumen, where the presence of NESP within the bitumen matrix acts as barriers to the deterioration of the bitumen structure, resulting in enhanced thermal stability of the bitumen. Like the penetration test, the softening point can also function as an indicator of high-temperature performance. A higher softening point suggests superior high-temperature performance, consequently reducing pavement

deterioration caused by permanent deformation [67].

3.3.5. Viscosity results

Fig. 8 illustrates the viscosity results at 135 °C and 165 °C. For both temperatures, the NESP-modified bitumen samples exhibited higher viscosities than the control sample. At 135 °C, the viscosity increased with rising NESP content. The recorded results for NESP were 0.606, 0.680, 0.720, 0.790, 0.841, and 0.925 Pa·s for 0%, 1%, 3%, 5%, 7%, and 9% NESP, respectively. The viscosity decreased as the test temperature was raised to 165 °C, with recorded viscosity values of 0.221, 0.230, 0.241, 0.255, 0.263, and 0.282 Pa·s for 0%, 1%, 3%, 5%, 7%, and 9% NESP, respectively. The increase in viscosity is attributed to the incorporation of NESP, resulting in an increase in the flow resistance of the modified bitumen. This is due to the formation of an intercalated structure, where the nanomaterial restricts the movement of bitumen molecules [5,66]. The increase in viscosity indicates that NESP can enhance the performance of bitumen in terms of resistance to permanent deformation and moisture [68].

The relationship between viscosity and temperature for control and NESP-modified bitumen samples is illustrated in Fig. 9. Based on this relationship, the temperatures for mixing and compacting were determined using viscosity standards of 0.17 ± 0.02 Pa·s for mixing and 0.28 ± 0.03 Pa·s for compacting [69,70]. Table 4 presents the mixing and compaction temperatures for both control and NESP-modified bitumen samples. It is evident that the mixing and compaction temperatures for NESP-modified bitumen samples were higher than those for the control sample. The high viscosity of the bitumen resulted in an increase in mixing and compaction temperatures, which will increase costs due to increased energy consumption. However, the increased cohesion of the bitumen may lead to improved adhesion between the bitumen and aggregates, thereby enhancing the performance of the asphalt mixture and reducing maintenance costs.

3.3.6. Temperature susceptibility results

In road construction, the recommended PI range for bitumen is -1.0 to $+1.0$ [71]. A high PI value, approaching the positive range, indicates low susceptibility to high temperatures and can enhance resistance against permanent deformation [71,72]. The results of the PI are depicted in Fig. 10. The PI for the modified samples increased from -0.9 for the control sample to -0.11 for the 9% NESP-modified bitumen sample and remained within the -1 to $+1$ range. This indicates that NESP significantly contributes to reducing bitumen sensitivity to high temperatures and enhancing its viscoelastic properties.

Fig. 11 presents the PVN results for both the control and NESP-modified bitumen samples. PVN results provide a similar indication to the PI. The NESP-modified bitumen samples displayed higher PVN values compared to the control samples, falling within the standard range of -2 to 0.5 , which is widely accepted in road construction [71]. A

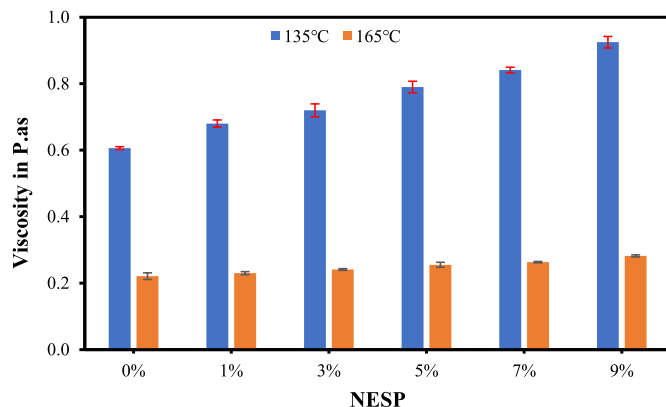


Fig. 8. Viscosity values for control and NESP-modified bitumen.

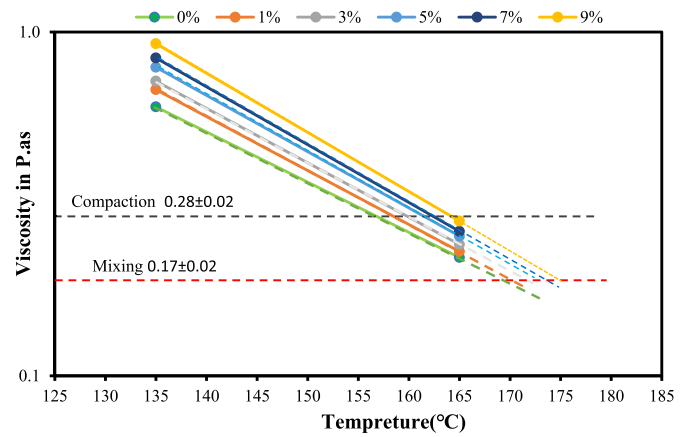


Fig. 9. The relationship of viscosity and temperature for control and NESP-modified bitumen.

Table 4

Mixing and compaction temperature for control and NESP-modified bitumen.

NESP (%)	Temperature (°C)	
	Mixing	Compaction
0.0	168	156
1.0	169	158
3.0	170	159
5.0	171	161
7.0	172	162
9.0	173	163

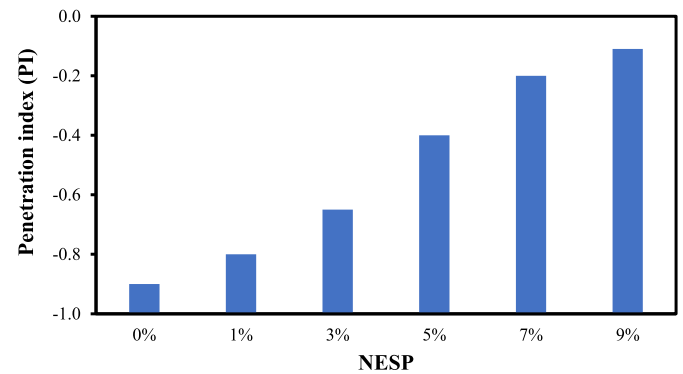


Fig. 10. Penetration index (PI) for control and NESP-modified bitumen.

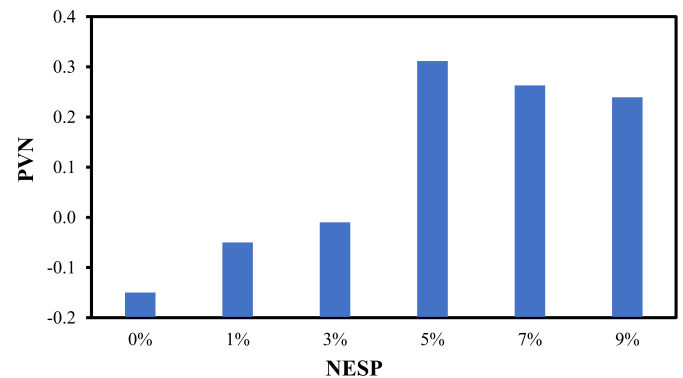


Fig. 11. Penetration-viscosity number (PVN) for control and NESP-modified bitumen.

lower PVN indicates greater temperature susceptibility [72]. Given that the PVN of the NESP-modified bitumen samples exceeded that of the control sample, it suggests that the NESP-modified bitumen samples are less sensitive to temperature.

3.3.7. Ductility results

Fig. 12 illustrates the ductility results for both control and NESP-modified bitumen. The ductility values of NESP-modified bitumen decreased by 2.5%, 5.8%, 8.3%, 13.2%, and 20% for 1%, 3%, 5%, 7%, and 9% NESP, respectively, compared to the control bitumen. The decrease in ductility could be attributed to the formation of strong bonds between the NESP and the bitumen matrix. These bonds increase the cohesiveness and stiffness of the bitumen, consequently leading to lower ductility in the modified bitumen compared to the control bitumen. One of the parameters used to characterize the low-temperature performance of bitumen is ductility [26]. The ductility results indicated that as the NESP content increased, the ductility of the bitumen decreased. However, the decrease was small and still within the range necessary to meet the specification requirements, which is more than 100 cm [43]. This suggests that NESP has a limited effect on low-temperature performance.

3.3.8. Mass loss after RTFO results

Mass loss is an indicator of bitumen ageing that may occur during the mixing and construction processes [73]. The results in Fig. 13 indicate that the control sample had the highest mass loss at 0.99% among all tested samples, and this value decreased with the addition of NESP. Specifically, 1%, 3%, 5%, 7%, and 9% NESP demonstrated mass losses of 0.68%, 0.67%, 0.60%, 0.53%, and 0.50%, respectively. NESP-modified bitumen exhibited lower mass loss, indicating that this incorporation reduced the volatility of bitumen components. This reduction in oxidation and volatilization could be attributed to the nanometric scale of NESP, which fill the porosity of the bitumen on a nanometric scale, enhancing impermeability and thereby mitigating the effects of oxidation and volatilization [74]. Moreover, the high surface area of NESP absorbed the lighter fractions of bitumen, thereby preventing volatilization after heating [5,66]. Therefore, the addition of NESP can contribute to delaying short-term aging and, consequently, extending the life of the modified binder. This finding aligns with previous studies showing that the addition of nanoparticles can reduce short-term bitumen aging [68,75,76].

3.3.9. DSR results

Fig. 14 shows the viscoelastic characteristics for both control and NESP-modified bitumen for unaged samples. It is evident from the figure that the NESP-modified bitumen had a higher complex modulus (G^*) than the control bitumen. This indicates that the NESP-modified bitumen samples exhibited greater stiffness and resistance to rutting in

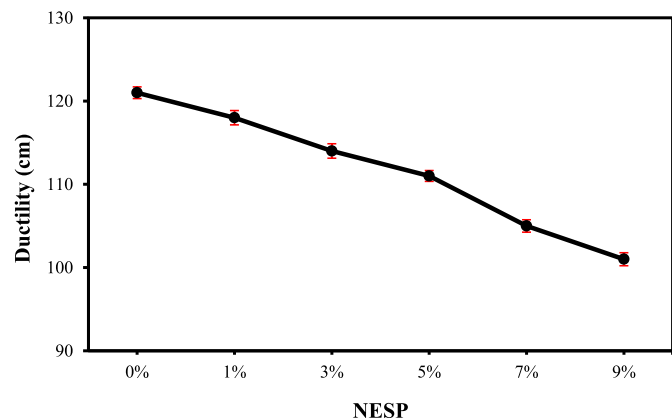


Fig. 12. Ductility value for control and NESP-modified bitumen.

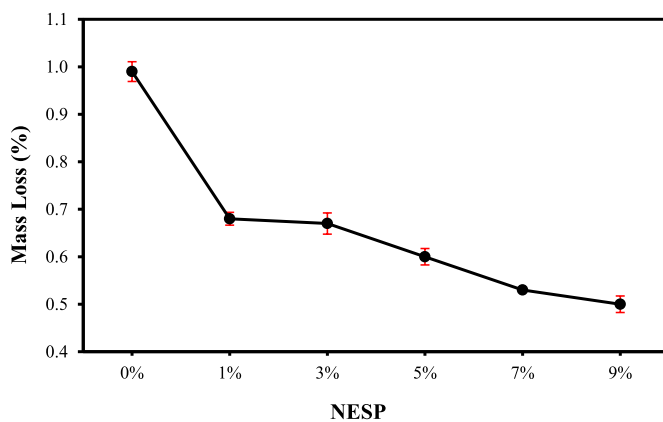


Fig. 13. The mass loss for control and NESP-modified bitumen.

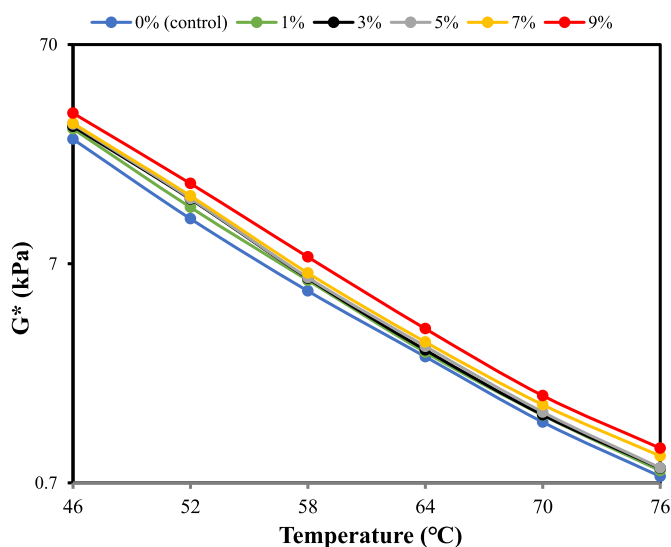


Fig. 14. $|G^*|$ for control and NESP-modified bitumen (unaged).

comparison to the control bitumen. Conversely, in Fig. 15, the phase angle (δ) of the NESP-modified bitumen samples was lower than that of the control bitumen. The phase angle indicates the percentage of viscoelastic elements in bitumen. Typically, a higher phase angle implies a higher proportion of viscous components and a lower capacity for

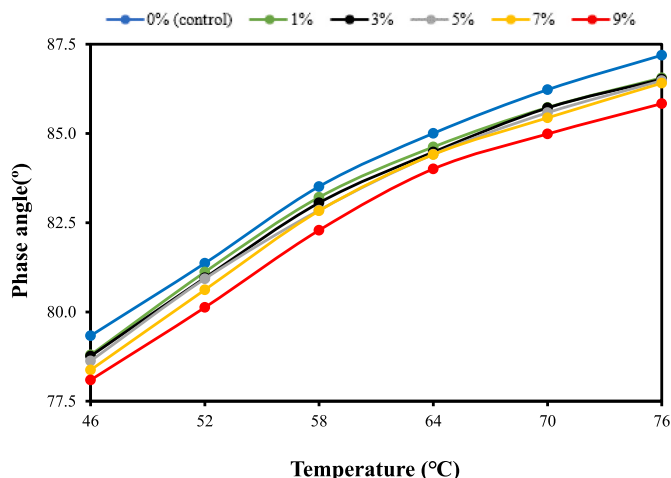


Fig. 15. Phase angle (δ) for control and NESP-modified bitumen (unaged).

deformation recovery [25]. As the temperature increases, the value of δ for bitumen also increases. In other words, as the temperature rises, the proportion of the viscous component in the bitumen increases, leading to a higher percentage of unrecoverable deformation. At the same time, the resistance to high-temperature deformation decreases. One potential reason could be that as the temperature increases, the bitumen becomes softer. When considering the same temperature, the value of δ decreases as the NESP content increases. Within the given temperature range, the reduction in δ compared to the control bitumen reaches its maximum extent at 9% NESP. The enhancement of bitumen resilience is achieved through the reduction of the phase angle. The decrease in the phase angle (δ) in NESP-modified bitumen can be attributed to the high surface area of NESP, which strengthens the connections between bitumen particles and forms a protective cover. This cover helps counteract the viscous behavior of bitumen at elevated temperatures, thus delaying the transition from elastic to viscous behavior [77]. This suggests that NESP enhances the bitumen's ability to recover after deformation.

Fig. 16 displays the rutting parameter, $|G^*|/\sin\delta$, for both the control and NESP-modified bitumen. The results reveal that rutting resistance is significantly affected by the NESP content, and there is a consistent trend of decreased rutting resistance with increasing test temperatures. The optimum improvement of 1.0 kPa was achieved with 9% NESP at 76 °C, with higher ($|G^*|/\sin\delta$) values recorded at all testing temperatures. This finding aligns with previous results for G^* and δ , where NESP improved the stiffness and elasticity of the bitumen. This indicates that the NESP-modified bitumen exhibits a higher performance grade compared to the control bitumen and can effectively resist permanent deformation or rutting at higher temperatures compared to unmodified bitumen. This improvement can be attributed to the large surface area of the nano-sized particles, which facilitated strong interfacial interactions between the NESP particles and the bitumen. As a result, stiffness and elasticity were enhanced, consequently improving the rutting performance of the bitumen. On the other hand, high temperatures have a significant impact on bitumen properties, and the variation in material stiffness depends on temperature susceptibility [78]. In general, the control bitumen exhibits high temperature sensitivity.

Further analysis was conducted using the RTFO samples to simulate the short-term aging process that occurs during the mixing and compaction of hot mix asphalt (HMA). The DSR results for both the control and NESP-modified bitumen samples are presented in Fig. 17, Fig. 18, and Fig. 19. The results clearly demonstrate substantially higher values of G^* for the aged samples compared to the unaged ones. Notably,

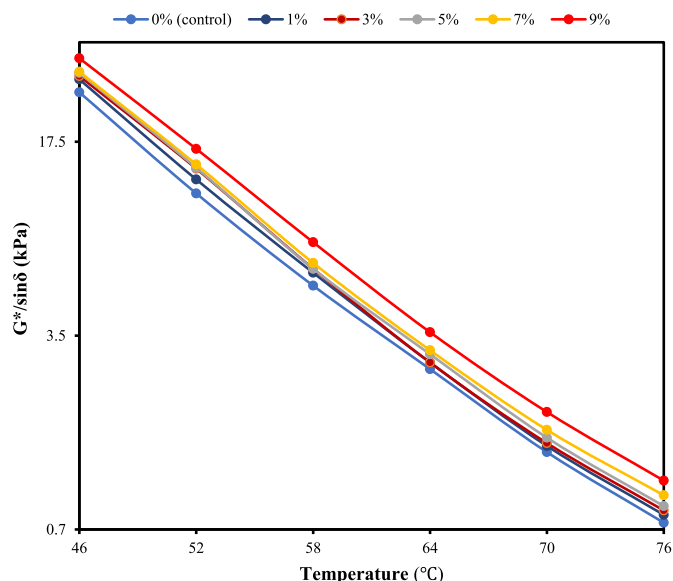


Fig. 16. $|G^*|/\sin\delta$ for control and NESP-modified bitumen (unaged).

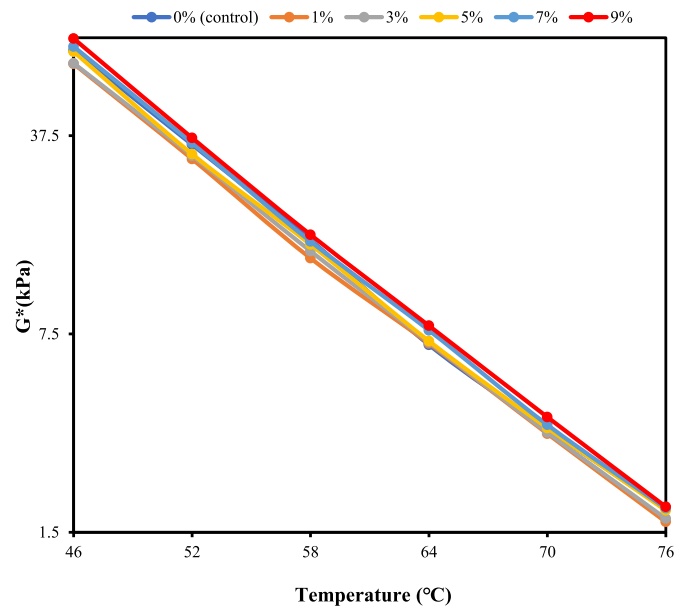


Fig. 17. $|G^*|$ for control and NESP-modified bitumen (RTFO-aged).

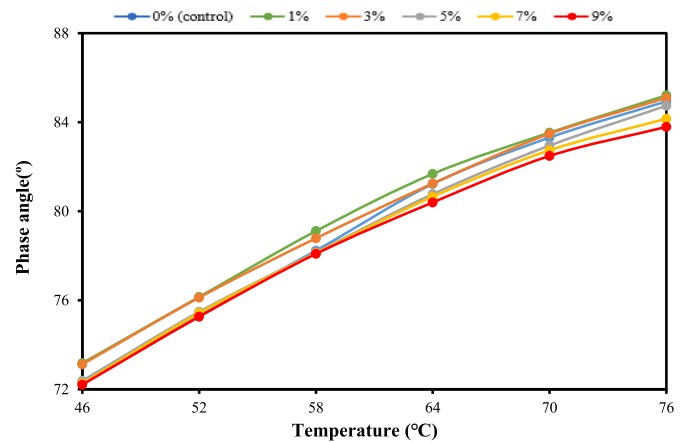


Fig. 18. Phase angle (δ) for control and NESP-modified bitumen (RTFO-aged).

9% NESP exhibited the highest G^* and the lowest (δ) value. As for the control bitumen, there was a significant increase in G^* compared to the unaged samples. This increase may be attributed to the higher loss of light materials after aging, as mentioned earlier; the control bitumen exhibited the highest mass loss among all samples. On the other hand, the increase in G^* for NESP-modified bitumen samples was moderate compared to unaged samples.

Fig. 19 displayed a similar pattern, with 9% NESP exhibiting the highest rutting resistance. It is evident that the control bitumen sample showed a significant increase in rutting resistance, attributed to the heightened hardness resulting from a rapid oxidation rate and the loss of oily materials after the heating process. In contrast, the NESP-modified bitumen samples demonstrate their capacity to maintain their performance grade by resisting rutting up to 70 °C after the short-term aging process. This suggests that NESP-modified bitumen samples do not undergo rapid hardening or oxidation due to the aging process. Consequently, the reduced susceptibility to aging may enhance the performance of asphalt mixtures in pavement by improving resistance to fatigue, thermal cracking, and deterioration caused by moisture [18].

Based on the results from the unaged and short-term aging samples, Fig. 20 displays the continuous grade findings for NESP-modified bitumen, illustrating the influence of NESP on the high-temperature

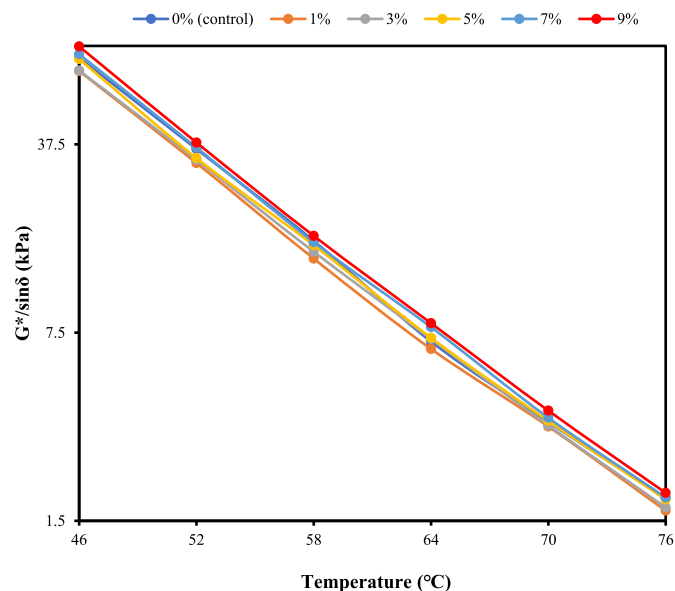


Fig. 19. $|G^*/\sin\delta|$ for control and NESP-modified bitumen (RTFO-aged).

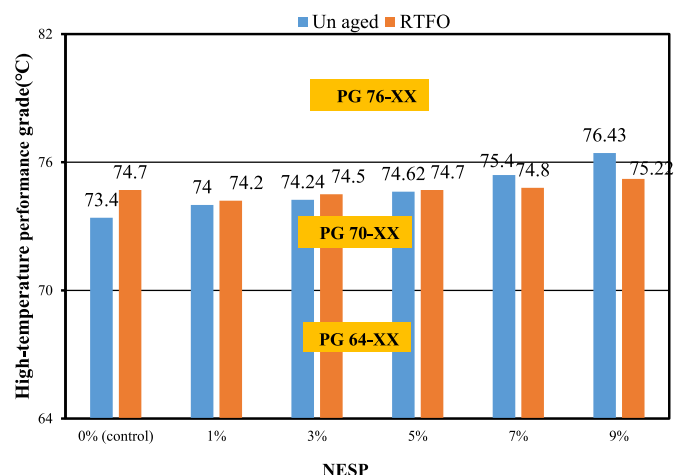


Fig. 20. High-temperature performance grade for control and NESP-modified bitumen.

performance grade of bitumen. As demonstrated in the figure, the addition of NESP to the bitumen gradually enhances the continuous grade, with unaged samples showing the most substantial gains. There is an increase of around 6 °C (PG 76-XX) for 9% NESP compared to the control bitumen. For the short-term aged samples, a constant increase in the continuous grade was also observed, albeit with a smaller magnitude, as 9%NESP causes a 5.2 °C increase in the continuous grade. The aged bitumen obtains the classification of PG70-XX.

3.3.10. Rutting factor aging index (RAI)

The Rutting Factor Aging Index (RAI) is a measure of the impact of aging conditions on the high-temperature performance of bitumen. It is calculated by comparing the ratio of $(G^*/\sin\delta)$ before and after aging, as demonstrated in equation (3) [66]. This index helps quantify how aging affects the bitumen ability to withstand rutting at elevated temperatures. As the RAI increases, the impact of aging becomes more noticeable [79].

$$RAI = \frac{(G^*/\sin\delta)_{aged}}{(G^*/\sin\delta)_{unaged}} \quad (3)$$

Fig. 21 illustrates the Rutting Aging Index (RAI) results for both the

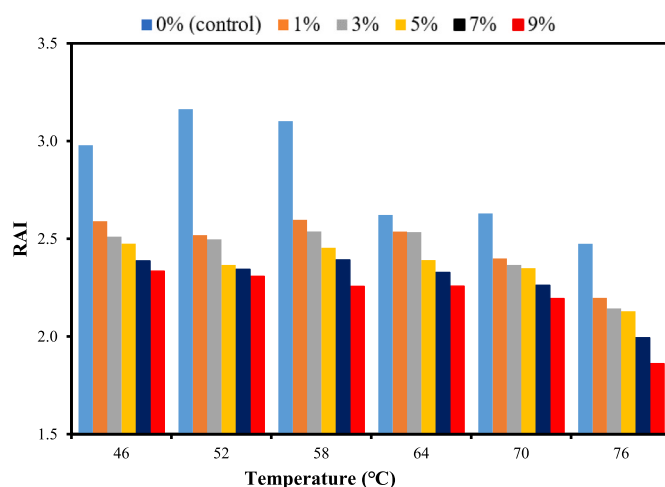


Fig. 21. Aging index (RAI) for control and NESP-modified bitumen.

NESP-modified bitumen and control samples. The results indicate that the control sample exhibited the highest RAI for all testing temperatures. Therefore, there is clear evidence that NESP contributes to the improvement of bitumen oxidation resistance. This phenomenon can be attributed to the presence of NESP particles, which mitigate the oxidation process by effectively distributing heat within the bitumen. The larger surface area of NESP enables more efficient heat absorption and distribution compared to control bitumen, which absorbs heat at a higher rate, resulting in accelerated bitumen aging and stiffness [1]. Additionally, NESP demonstrates high-temperature stability, maintaining its performance throughout the heating process. This stability is attributed to its high CaCO_3 content [48,80]. Furthermore, the nano-scale dimensions of NESP enable it to fill nanopores, enhancing the impermeability of the bitumen and reducing its susceptibility to oxidation and volatilization [68]. Moreover, the substantial specific surface area and surface energy of the nanomaterial ensure an increased adsorption level within the matrix, preventing the leakage of oily components from the bitumen, as they adhere to the solid surface of nanoparticles [5,18,68].

3.3.11. Fourier transform infrared (FTIR) results

The Fourier Transform Infrared (FTIR) spectra are capable of analyzing and identifying changes in the functional groups of bitumen materials and investigating the aging of bitumen [24,25]. The FT-IR spectra in the range of $4000\text{--}500\text{ cm}^{-1}$ wavenumber for the control and NESP-modified bitumen are shown in Fig. 22. The infrared spectra of bitumen materials reveal three prominent absorption peaks [5,25, 81–83]. In Section I of the spectra, bitumen exhibits significant absorption peaks located at approximately 2920.14 cm^{-1} and 2851.53 cm^{-1} , attributed to the stretching vibrations of aliphatic chains of C–H bonds, both symmetrical and asymmetrical (methylene $-\text{CH}_2-$ and methyl CH_3-), present within the bitumen materials. In section II, the bitumen material exhibits the second highest peaks at around 1456.83 cm^{-1} and 1375.94 cm^{-1} . These peaks are primarily attributed to the bending vibration of $-\text{CH}_2$ and $-\text{CH}_3$ groups, and the vibration peaks generated by CO_3^{2-} from the NESP. The absorption peaks observed at 861.25 cm^{-1} , 809.37 cm^{-1} , 745.12 cm^{-1} , and 722.54 cm^{-1} in section III could potentially be attributed to the bending vibration of the C–H bond in aromatic compounds, along with the vibration peaks caused by the presence of CO_3^{2-} introduced through the addition NESP.

The wavenumber range of $2000\text{--}600\text{ cm}^{-1}$ is where the functional groups show the most prominent variations in chemical composition [84,85]. As a result, the analysis primarily centred on examining these functional groups within this specific range. A low peak at 1700 cm^{-1} ($\text{C}=\text{O}$) was observed after the modification of the bitumen due to the

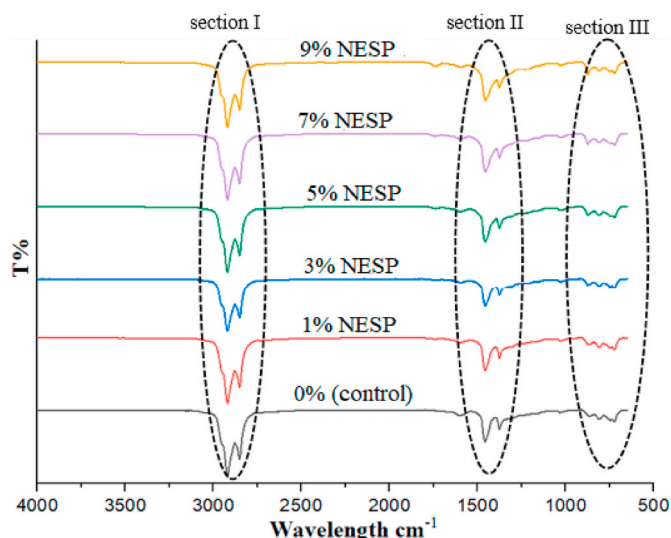


Fig. 22. FTIR spectra of control and NESP-modified bitumen.

introduction of CO_3^{2-} through the addition of NESP. As the concentration of NESP increased, the aromatic bonds ($\text{C}=\text{C}$) at 1600 cm^{-1} decreased. The aromatic index $[\text{A}_{1600}/\Sigma_{(\text{peak zone area between } 2000\text{cm}^{-1}\text{ and } 600\text{cm}^{-1})}]$ decreased from 0.06 in the control bitumen to 0.0485, 0.047, 0.0468, 0.0454, and 0.037 for 1%, 3%, 5%, 7%, and 9% NESP, respectively, as shown in Fig. 23. Conversely, the aliphatic index $[(\Sigma \text{A}_{1452+\text{A}_{1373}})/\Sigma_{(\text{peak zone area between } 2000\text{cm}^{-1}\text{ and } 600\text{cm}^{-1})}]$ were increased with the increase in NESP concentration. The aliphatic index increased from 0.42 in the control bitumen to 0.458, 0.54, 0.541, 0.572, and 0.573 for 1%, 3%, 5%, 7%, and 9% NESP, respectively, as shown in Fig. 23.

The aromatic and aliphatic index are useful indicators for understanding the aging mechanisms. Previous research suggests that aging reactions can be identified when the aromatic index increases and the aliphatic index decreases [85–88]. This indicates that the addition of the NESP to the bitumen retarded the oxidation process.

3.3.12. AFM results

AFM was utilized to evaluate the roughness of control bitumen and NESP-modified bitumen with 5%, 7%, and 9%. The topography of

bitumen is divided into three phases: bee structure (peaks and valleys), dispersed domain (dark color region), and flat matrix (light color region) [86]. According to Fig. 24, the size of bee structures decreased as the NESP content increased. The 9% NESP-modified bitumen exhibited the smallest bee structures and most homogeneously dispersed domains. The reduction in the size of bee structures in NESP-modified bitumen can be justified by considering the composition of bitumen. Bitumen is a complex mixture containing various components, and differences in these components result in significant variations in the nano-microstructure [89]. It consists of polar components such as asphaltenes and colloids (which constitute the bee structure), as well as nonpolar components comprising saturated and aromatic compounds [90]. During the process of modifying bitumen, which occurs at high temperatures and under shear forces, the polar components of bitumen are melted and dispersed. As the temperature drops, NESP creates a stable network structure within the bitumen matrix [91]. This prevents the attraction of polar compounds to each other after dispersion, thereby inhibiting the formation of high molecular structures.

To better analyze the evolution characteristics of the nano-microstructure of bitumen, Rq and Ra were selected to quantify the differences in nano morphologies. Fig. 25 illustrates the roughness parameters of bitumen with varying NESP dosages. The nano roughness of bitumen undergoes significant changes as NESP content increases, as depicted in Fig. 25. Compared to the control bitumen, the Rq and Ra values of the NESP-modified bitumen decrease, consistent with the phenomenon depicted in Fig. 24, where the size of the bee-like structure decreases with increased NESP content.

Rq plays a crucial role in adhesion as it accounts for the surface's peaks and valleys. Peaks hinder the bonding of two different materials, thus reducing adhesion at peak locations [92]. Therefore, these findings indicate that the performance of the asphalt mixture will be enhanced by improving the adhesion between the modified bitumen and aggregates.

3.3.13. Contact angle results

A contact angle test was performed to investigate the effect of NESP on bitumen adhesion properties. The surface of non-polar materials like bitumen typically exhibits limited spreading of polar materials such as water. Fig. 26 demonstrates that incorporating NESP resulted in a decrease in the contact angle observed between distilled water and bitumen. The average contact angles measured were 99.2° , 98.5° , 96.5° , 92.2° , 88.8° , and 86.4° for the control, 1%, 3%, 5%, 7%, and 9% NESP,

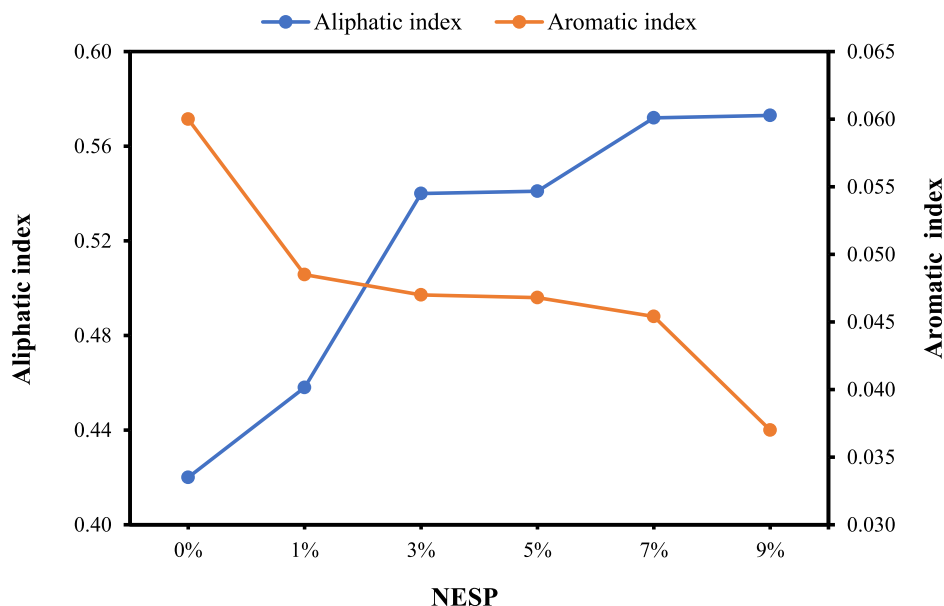


Fig. 23. Aromatic and aliphatic index for control and NESP-modified bitumen.

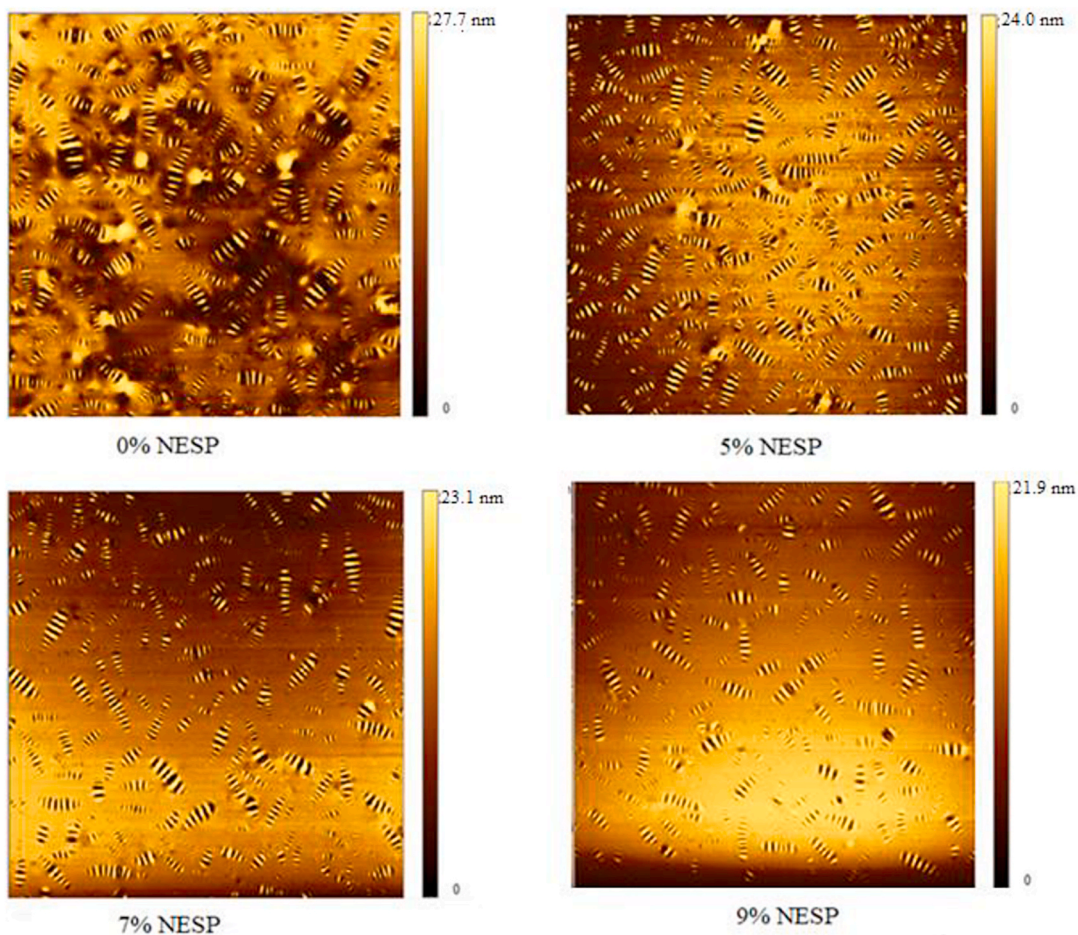


Fig. 24. Topography of control and NESP-modified bitumen scale (50µm * 50µm).

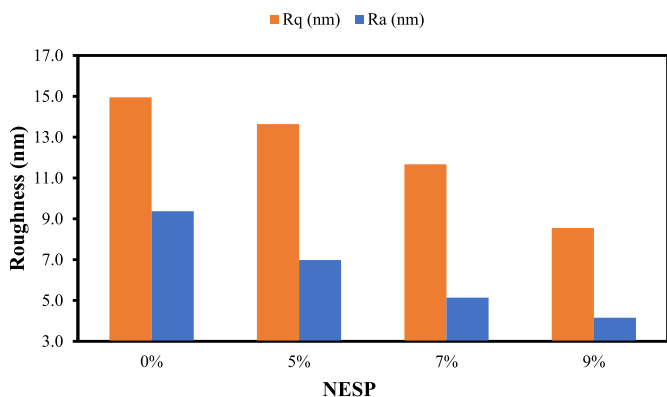


Fig. 25. Value of roughness (Ra, Rq) for control and NESP-modified bitumen.

respectively. The decrease in the contact angle indicates enhanced wetting ability of the bitumen. Thus, incorporating NESP can enhance the adhesion between the bitumen and aggregates. Improved adhesion can enhance the performance of asphalt mixtures, particularly in terms of high temperatures and resistance to moisture damage. This could be attributed to the fact that NESP is an alkaline substance, due to its high calcium carbonate content. As a result, it may enhance the basic component of the surface free energy (SFE) of the bitumen, resulting in a greater capacity for chemical interaction between the bitumen and mineral aggregates. Similar findings were reported by Manfro et al. [74] wherein the incorporation of nano CaCO₃ improved the adhesion between bitumen and aggregate.

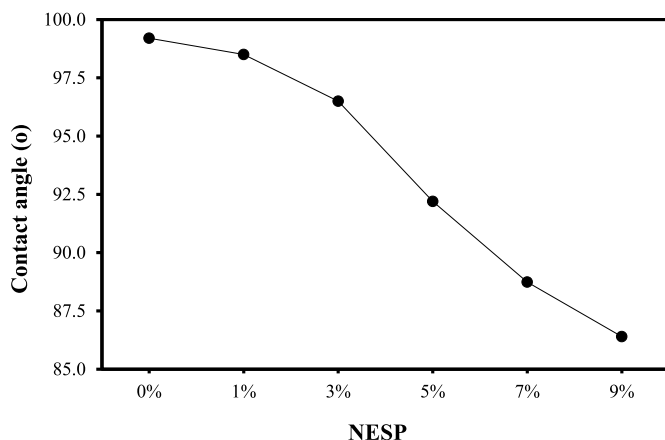


Fig. 26. Contact angle for control and NESP-modified bitumen.

3.3.14. Thermogravimetric analysis results

Fig. 27(a) and (b) display the TGA and DTG analyses of the control and NESP-modified bitumen. The TGA curves reveal three distinct regions. The initial phase represents the elimination of moisture and light volatiles, known as the drying phase. The second phase shows a consistent mass loss with increasing rates, indicating the thermal decomposition of components within the bitumen. The third region demonstrates a sublimation process, characterized by ongoing mass loss at a diminishing rate [93].

The DTG curve provides information on the rate of mass loss change

with temperature, facilitating the determination of the temperature at which this rate reaches its maximum [94]. The initial section of the DTG curve, where the rate of mass loss is nearly zero, corresponds to the section of the TGA curve with minimal mass loss. Mass loss gradually increases in the thermal decomposition region until reaching a temperature where the rate of mass loss peaks.

According to the results in Fig. 27(a), the control bitumen undergoes more weight loss during the test compared to the NESP-modified bitumen. Additionally, modified bitumen with lower NESP concentrations experiences more weight loss than samples with a higher proportion of NESP. These findings suggest that NESP modified bitumen exhibits less evaporation and greater thermal stability compared to control bitumen.

The parameters epitaxial decomposition temperature (T_{ed}), the fastest decomposition temperature (T_m), and the percentage of final residual mass (M_f) for control and NESP-modified bitumen are presented

Table 5
The T_{ed} , T_m , and M_f o for control and NESP-modified bitumen.

NESP (%)	$T_{ed}/^{\circ}\text{C}$	$T_m/^{\circ}\text{C}$	$M_f/\%$
0.0	350.1	440.95	16.96
1.0	360.1	447.25	17.36
3.0	361.8	449.65	18.99
5.0	363.2	450.15	20.3
7.0	367.3	450.5	22.29
9.0	368.0	451.45	22.99

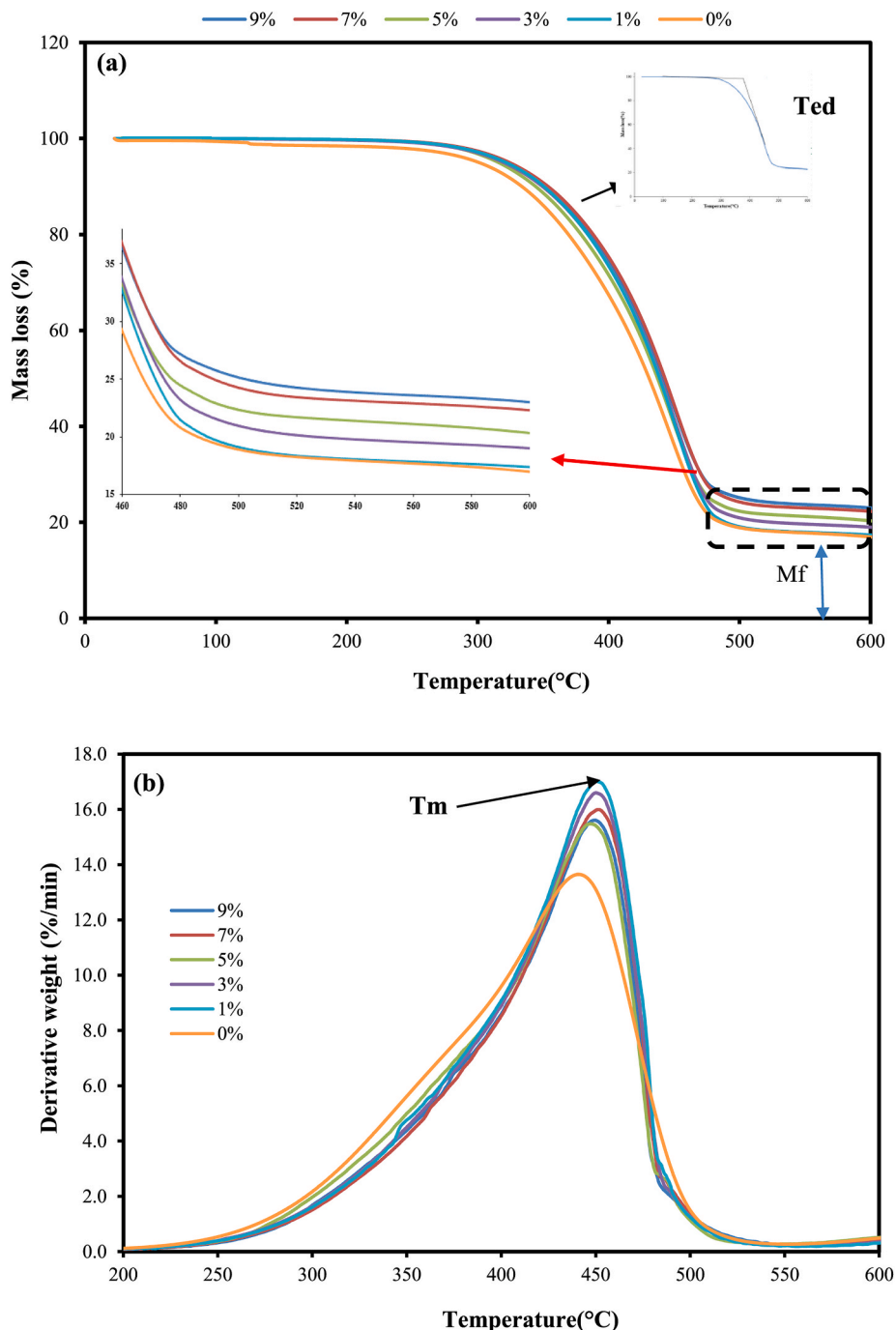


Fig. 27. (a) TGA and (b) DTG analysis for control and NESP-modified bitumen.

in Table 5. In general, it was observed that the addition of NESP increased the T_{ed} , T_m , and M_f , indicating that the NESP enhanced the thermal stability of bitumen. The improved performance of modified bitumen is attributed to the additive of NESP with a high content of CaCO_3 , which has a decomposition temperature around 700–750 °C [95], helping to elevate the thermal stability of NESP-modified bitumen. Moreover, as mentioned earlier, the substantial surface area of NESP plays a crucial role in mitigating the oxidation process by efficiently dispersing heat within the bitumen. The larger surface area of NESP allows for more effective heat absorption and distribution in comparison to control bitumen, which absorbs heat at a higher rate. Therefore, NESP can enhance the performance of bitumen at high temperatures and reduce susceptibility to permanent deformation.

4. Conclusions, recommendations, and concerns

This study investigates the effect of nano-sized eggshell waste on the physical, rheological properties, and microstructure characteristics of bitumen. The results offer additional theoretical support for the application of eggshell waste in bio-roads, which is critical for society and the economy. The following are the key conclusions.

- NESP was compatible with bitumen, as evidenced by the storage stability results. Moreover, XRD patterns for the NESP-modified bitumen revealed an inorganic modification associated with the crystalline structure of NESP, indicating a well dispersion of NESP in the bitumen matrix.
- NESP improves the hardness, cohesion, and viscosity of bitumen while decreasing ductility.
- The DSR temperature sweep results demonstrated that NESP could increase the resistance of bitumen to rutting and aging.
- NESP improves the adhesion properties of bitumen by increasing its wettability and reducing the nano surface roughness through alterations in the maturity, size, and quantity of the ‘bee-like structure’.
- NESP improved the thermal stability of bitumen, as evidenced by TGA analysis.
- The highest improvement in the physical and rheological properties of bitumen was achieved with a 9% NESP content.

Overall, the addition of NESP has a significant effect on the high-temperature characteristics of bitumen. Therefore, it is recommended for use in hot environments, particularly in the surface layer, which is the primary layer exposed to traffic loads and environmental variations. For future research, we recommend.

- Assessing the medium and low-temperature performance of NESP-modified bitumen. Moreover, investigating the mechanical properties of asphalt mixtures containing NESP would offer a more comprehensive understanding of NESP effect on pavement materials.
- Future research should focus more on understanding the interaction mechanism between biological waste and bitumen.
- It would also be meaningful to develop nanomaterials derived from other biomaterial waste, which could effectively enhance various properties of bitumen.

Prior to the practical application of NESP-modified bitumen in the production and construction process, it is reasonable to anticipate that collecting a significant amount of eggshell waste from a single location could pose challenges due to potential cost concerns [26]. However, utilizing it as modifier for bitumen can enhance the recycling of solid waste and decrease the dependency on petroleum products. Therefore, it is essential to evaluate their benefits by emphasizing these advantages rather than solely focusing on the cost factor. For example, in Malaysia, approximately 642,600 tonnes of eggs are produced annually, resulting in an expected generation of about 70,686 tons of eggshell waste per year [40]. This amount can potentially produce about 700,000 tons of

NESP-modified bitumen annually (with a 10% addition of NESP). This modified bitumen can be utilized for paving or maintenance purposes. Therefore, it is imperative to devise appropriate strategies, enact legislation, and establish standardized procedures to effectively utilize it.

CRediT authorship contribution statement

Alattafi Hadi Zghair Chfat: Writing – original draft. **Haryati Yaacob:** Writing – review & editing. **Nurul Hidayah Mohd Kamaruddin:** Visualization. **Zaid Hazim Al-Saffar:** Writing – review & editing. **Ramadhansyah Putra Jaya:** Visualization.

Declaration of competing interest

The authors declare that they have no known competing financial interests or personal relationships that could have appeared to influence the work reported in this paper.

Data availability

Data will be made available on request.

References

- [1] S.N.A. Jeffry, R.P. Jaya, N.A. Hassan, H. Yaacob, J. Mirza, S.H. Drahman, Effects of nanocharcoal coconut-shell ash on the physical and rheological properties of bitumen, *Construct. Build. Mater.* 158 (2018) 1–10.
- [2] A. Abouelsaad, G. White, A. Jamshidi, State of the art review of ageing of bituminous binders and asphalt mixtures: ageing simulation techniques, ageing inhibitors and the relationship between simulated ageing and field ageing, *Infrastructure* 9 (1) (2024) 8. <https://www.mdpi.com/2412-3811/9/1/8>.
- [3] A.Y. Aboelmagd, G.S. Moussa, M. Enieb, S. Khedr, E.-S.M. Abd Alla, Evaluation of hot mix asphalt and binder performance modified with high content of nano silica fume, *JES. Journal of Engineering Sciences* 49 (4) (2021) 378–399.
- [4] G.A. Shafabakhsh, M. Sadeghnejad, S. Alizadeh, Engineering the effect of nanomaterials on bitumen and asphalt mixture properties. A review, *Baltic J. Road Bridge Eng.* 18 (2) (2023) 1–31.
- [5] W.B. Broering, J.V.S. de Melo, A.L. Manfro, Incorporation of nanoalumina into a polymeric asphalt matrix: reinforcement of the nanostructure, improvement of phase stability, and amplification of rheological parameters, *Construct. Build. Mater.* 320 (2022) 126261, <https://doi.org/10.1016/j.conbuildmat.2021.126261>, 2022/02/21/.
- [6] J. Zhu, B. Birgisson, N. Kringos, Polymer modification of bitumen: advances and challenges, *Eur. Polym. J.* 54 (2014) 18–38.
- [7] C. Fang, R. Yu, S. Liu, Y. Li, Nanomaterials applied in asphalt modification: a review, *J. Mater. Sci. Technol.* 29 (7) (2013) 589–594, <https://doi.org/10.1016/j.jmst.2013.04.008>, 2013/07/01/.
- [8] Y. Erkuş, B.V. K k, Comparison of physical and rheological properties of calcium carbonate-polypropylene composite and SBS modified bitumen, *Construct. Build. Mater.* 366 (2023) 130196.
- [9] N. Xu, H. Wang, Y. Chen, M. Miljkovi c, P. Feng, H. Ding, Thermal storage stability and rheological properties of multi-component styrene-butadiene-styrene composite modified bitumen, *Construct. Build. Mater.* 322 (2022) 126494.
- [10] J. Liu, K. Yan, W. Liu, X. Zhao, Partially replacing Styrene-Butadiene-Styrene (SBS) with other asphalt binder modifier: feasibility study, *Construct. Build. Mater.* 249 (2020) 118752.
- [11] W. Zhang, et al., Evaluation method of storage stability of SBS modified bitumen based on dynamic rheological properties, *Construct. Build. Mater.* 323 (2022) 126615.
- [12] Y.M. Alghrafy, E.-S.M. Abd Alla, S.M. El-Badawy, Phase angle master curves of sulfur-extended asphalt modified with recycled polyethylene waste, *Innovative Infrastructure Solutions* 6 (2021) 1–11.
- [13] Z. Ji, L. Sun, L. Chen, W. Gu, Y. Tian, X. Zhang, Pavement performance and modification mechanisms of asphalt binder with nano- Al_2O_3 , *Int. J. Pavement Eng.* (2022) 1–11.
- [14] T. Abdel-Wahed, A. Abdel-Raheem, G. Moussa, Performance evaluation of asphalt mixtures modified with nanomaterials, *MEJ. Mansoura Engineering Journal* 47 (1) (2022) 1–15.
- [15] F. Ameen, K. Alsamhary, J.A. Alabdullatif, S. AlNadhari, A review on metal-based nanoparticles and their toxicity to beneficial soil bacteria and fungi, *Ecotoxicol. Environ. Saf.* 213 (2021) 112027.
- [16] W.J. Steyn, Applications of nanotechnology in road pavement engineering, *Nanotechnology in civil infrastructure: a paradigm shift* (2011) 49–83.
- [17] L.P. Santos, J. Crucho, Nano-Modified Asphalt Binders and Mixtures to Enhance Pavement Performance, MDPI, 2020.
- [18] N. Cadorn, J. Victor Staub de Melo, W. Borba Broering, A. Luiz Manfro, B. Salgado Barra, Asphalt nanocomposite with titanium dioxide: mechanical, rheological and photoactivity performance, *Construct. Build. Mater.* 289 (2021) 123178, <https://doi.org/10.1016/j.conbuildmat.2021.123178>, 2021/06/28/.

- [19] G.A. Shafabakhsh, M. Sadeghnejad, B. Ahoor, E. Taheri, Laboratory experiment on the effect of nano SiO₂ and TiO₂ on short and long-term aging behavior of bitumen, *Construct. Build. Mater.* 237 (2020) 117640, <https://doi.org/10.1016/j.conbuildmat.2019.117640>, 2020/03/20/.
- [20] S.A. Ghanoun, J. Tanzadeh, M. Mirsepahi, Laboratory evaluation of the composition of nano-clay, nano-lime and SBS modifiers on rutting resistance of asphalt binder, *Construct. Build. Mater.* 238 (2020) 117592.
- [21] A.M. Mohammed, A.H. Abed, Enhancing asphalt binder performance through nano-SiO₂ and nano-CaCO₃ additives: rheological and physical insights, *Case Stud. Constr. Mater.* 19 (2023) e02492, <https://doi.org/10.1016/j.cscm.2023.e02492>, 2023/12/01/.
- [22] J. Crucho, L. Picado-Santos, J. Neves, S. Capitão, A review of nanomaterials' effect on mechanical performance and aging of asphalt mixtures, *Appl. Sci.* 9 (18) (2019) 3657.
- [23] S. Lv, et al., Improvements on high-temperature stability, rheology, and stiffness of asphalt binder modified with waste crayfish shell powder, *J. Clean. Prod.* 264 (2020) 121745.
- [24] X. Yang, J. Mills-Beale, Z. You, Chemical characterization and oxidative aging of bio-asphalt and its compatibility with petroleum asphalt, *J. Clean. Prod.* 142 (2017) 1837–1847.
- [25] X. Wang, G. Ji, Y. Zhang, Y. Guo, J. Zhao, Research on high-and low-temperature characteristics of bitumen blended with waste eggshell powder, *Materials* 14 (8) (2021) 2020.
- [26] J. Huang, G. Shiva Kumar, J. Ren, Y. Sun, Y. Li, C. Wang, Towards the potential usage of eggshell powder as bio-modifier for asphalt binder and mixture: workability and mechanical properties, *Int. J. Pavement Eng.* 23 (10) (2022) 3553–3565.
- [27] G. Fan, et al., Analysis of the influence of waste seashell as modified materials on asphalt pavement performance, *Materials* 15 (19) (2022) 6788.
- [28] Y. Guo, X. Wang, G. Ji, Y. Zhang, H. Su, and Y. Luo, "Effect of recycled shell waste as a modifier on the high- and low-temperature rheological properties of asphalt," *Sustainability*, vol. 13, no. 18, doi: 10.3390/su131810271.
- [29] C. Hu, D. Zhong, S. Li, A study on effect of oyster shell powder on mechanical properties of asphalt and multiple degrees of modification mechanism, *Case Stud. Constr. Mater.* 18 (2023) e01786.
- [30] Y. Zhang, et al., Effect of bio-oil on rheology and chemistry of organosolv lignin-modified bitumen, *J. Mater. Civ. Eng.* 34 (4) (2022) 04022009.
- [31] S.A.S. Al Abri, C.R. Rollakanti, K.K. Pololu, A. Joe, Experimental study on mechanical properties of concrete by partial replacement of cement with eggshell powder for sustainable construction, *Mater. Today: Proc.* 65 (2022) 1660–1665.
- [32] F. Alsharari, et al., Sustainable use of waste eggshells in cementitious materials: an experimental and modeling-based study, *Case Stud. Constr. Mater.* 17 (2022) e01620.
- [33] M. Waheed, et al., Channelling eggshell waste to valuable and utilizable products: a comprehensive review, *Trends Food Sci. Technol.* 106 (2020) 78–90.
- [34] S. Owuamanam, D. Cree, Progress of bio-calcium carbonate waste eggshell and seashell fillers in polymer composites: a review, *J. Composites Sci.* 4 (2) (2020) 70. <https://www.mdpi.com/2504-477X/4/2/70>.
- [35] A. Francis, M.A. Rahman, The environmental sustainability of calcined calcium phosphates production from the milling of eggshell wastes and phosphoric acid, *J. Clean. Prod.* 137 (2016) 1432–1438.
- [36] K. Khan, W. Ahmad, M.N. Amin, A.F. Deifalla, Investigating the feasibility of using waste eggshells in cement-based materials for sustainable construction, *J. Mater. Res. Technol.* 23 (2023) 4059–4074.
- [37] P. Shekhawat, G. Sharma, R.M. Singh, Strength behavior of alkaline activated eggshell powder and flyash geopolymer cured at ambient temperature, *Construct. Build. Mater.* 223 (2019) 1112–1122.
- [38] Y. Zhang, et al., Waste eggshell membrane-assisted synthesis of magnetic CuFe₂O₄ nanomaterials with multifunctional properties (adsorptive, catalytic, antibacterial) for water remediation, *Colloids Surf. A Physicochem. Eng. Asp.* 612 (2021) 125874.
- [39] M. Amin, M.M. Attia, I.S. Agwa, Y. Elskhawy, K. Abu El-hassan, B.A. Abdelsalam, Effects of sugarcane bagasse ash and nano eggshell powder on high-strength concrete properties, *Case Stud. Constr. Mater.* 17 (2022) e01528.
- [40] M. Shahinuzzaman, et al., Carbon dioxide minimization using sodium and potassium impregnated calcium oxide sorbent derived from waste eggshell, *React. Kinet. Mech. Catal.* 137 (1) (2024) 359–374.
- [41] T. Syammaun, M. Isya, F. Rachman, Assessing the performance of eggshell ash as a sustainable bitumen modifier, *Transport Eng.* (2023) 100196.
- [42] L. Zani, F. Giustozzi, J. Harvey, Effect of storage stability on chemical and rheological properties of polymer-modified asphalt binders for road pavement construction, *Construct. Build. Mater.* 145 (2017) 326–335.
- [43] Standards & Industrial Research Institute of Malaysia (SIRIM), Specification for Penetration Grade of Bitumen for Use in Pavement Construction (First Revision), 1996. Kuala Lumpur, MS 124.
- [44] ASTM D5/D5M, Standard Test Method for Penetration of Bituminous Materials, ASTM International, USA, 2013.
- [45] ASTM D36/D36M, Standard Test Method for Softening Point of Bitumen (Ring-and-Ball Apparatus), American Association of State and Highway Transportation Officials, Washington, DC, 2014.
- [46] ASTM D4402/D4402M, Standard Test Method for Viscosity Determination of Asphalt at Elevated Temperatures Using a Rotational Viscometer 5–7, American Society for Testing and Materials, American Society for Testing and Materials, West Conshohocken, PA, United States, 1999, 2015.
- [47] ASTM D7175, "Standard Test Method for Determining the Rheological Properties of Asphalt Binder Using a Dynamic Shear Rheometer, ASTM International; 2015, West Conshohocken, USA, 2015. Annual Book of ASTM Standards.
- [48] H. Raufi, A. Topal, D. Kaya, B. Sengoz, Performance evaluation of nano-CaCO₃ modified bitumen in hot mix asphalt, in: *Proceedings of the 18th IRF World Road Meeting*, 2022, pp. 14–17. Delhi, India.
- [49] K. Debbarma, B. Debnath, P.P. Sarkar, A comprehensive review on the usage of nanomaterials in asphalt mixes, *Construct. Build. Mater.* 361 (2022) 129634, <https://doi.org/10.1016/j.conbuildmat.2022.129634>, 2022/12/26/.
- [50] ASTM-D5976, Standard Specification for Type I Polymer Modified Asphalt Cement for Use in Pavement Construction1, ASTM International., West Conshohocken, PA, USA, 2000.
- [51] E.R. Brown, P.S. Kandhal, F.L. Roberts, Y.R. Kim, D.-Y. Lee, T.W. Kennedy, *Hot Mix Asphalt Materials, Mixture Design, and Construction*, NAPA research and education foundation, 2009.
- [52] ASTM D113, Standard Test Method for Ductility of Bituminous Materials, ASTM International., West Conshohocken, PA, USA, 2017.
- [53] ASTM-D2872, Standard Test Method for Effect of Heat and Air on a Moving Film of Asphalt (Rolling Thin-Film Oven Test), Annual Book of ASTM Standards, ASTM International, West Conshohocken, USA, 2012. ASTM International; 2012.
- [54] Z.Y.M. Al-Hemedaoi, Effect of Liquefied Food Waste on Asphalt Mixture Performance, *Universiti Teknologi Malaysia*, 2021.
- [55] S. Nizamuddin, M. Jamal, R. Gravina, F. Giustozzi, Recycled plastic as bitumen modifier: the role of recycled linear low-density polyethylene in the modification of physical, chemical and rheological properties of bitumen, *J. Clean. Prod.* 266 (2020) 121988.
- [56] ASTM E1131, ASTM E1131. Standard Test Method for Compositional Analysis by Thermogravimetry, Annual Book of ASTM Standards, ASTM International, West Conshohocken, USA, 2014 (08) 2014.
- [57] S.S. Ciryale, P. Alexandre, C. Emmanuel, Evaluation of the potential use of waste sunflower and rapeseed oils-modified natural bitumen as binders for asphalt pavement design, *Int. J. Pavement Res. Technol.* 9 (5) (2016) 368–375.
- [58] B. Shu, S. Wu, L. Pang, B. Javilla, The utilization of multiple-walled carbon nanotubes in polymer modified bitumen, *Materials* 10 (4) (2017) 416.
- [59] L.Y.F. Ng, H. Ariffin, T.A.T. Yasim-Anuar, M.A.A. Farid, M.A. Hassan, High-energy ball milling for high productivity of nanobiochar from oil palm biomass, *Nanomaterials* 12 (18) (Sep 19 2022), <https://doi.org/10.3390/nano12183251> (in eng).
- [60] C. Prommalikit, W. Mekprasart, W. Pecharapa, Effect of milling speed and time on ultrafine ZnO powder by high energy ball milling technique, in: *Journal of Physics: Conference Series*, IOP Publishing, 2019 012023 vol. 1259, no. 1.
- [61] B. Wang, et al., Effect of milling time on microstructure and properties of Nano-titanium polymer by high-energy ball milling, *Appl. Surf. Sci.* 434 (2018) 1248–1256, <https://doi.org/10.1016/j.apsusc.2017.11.265>, 2018/03/15/.
- [62] M. Rijesh, M. Sreekanth, A. Deepak, K. Dev, A. Surendranathan, Effect of milling time on production of aluminium nanoparticle by high energy ball milling, *Int. J. Mech. Eng. Technol.* 9 (8) (2018) 646–652.
- [63] I.M. Nasser, M.H.W. Ibrahim, S.S.M. Zuki, A.F. Alsharif, N. Nindyawati, R.P. Jaya, Effects of milling time on nano rice husk ash particle size, in: *E3S Web of Conferences*, EDP Sciences, 2023 01003 vol. 445.
- [64] G.H. Hamed, F. Moghadas Nejad, Use of aggregate nanocoating to decrease moisture damage of hot mix asphalt, *Road Mater. Pavement Des.* 17 (1) (2016) 32–51.
- [65] H. Nazari, K. Naderi, F.M. Nejad, Improving aging resistance and fatigue performance of asphalt binders using inorganic nanoparticles, *Construct. Build. Mater.* 170 (2018) 591–602.
- [66] N.D.A. Cadornin, J.V.S. de Melo, W.B. Broering, A.L. Manfro, B.S. Barra, Asphalt nanocomposite with titanium dioxide: mechanical, rheological and photoactivity performance, *Construct. Build. Mater.* 289 (2021) 123178.
- [67] P. Sun, K. Zhang, Y. Xiao, Z. Liang, Analysis of pavement performance for nano-CaCO₃/SBS modified asphalt mixture, in: *Journal of Physics: Conference Series*, IOP Publishing, 2022 012031 vol. 2329, no. 1.
- [68] A.L. Manfro, J.V.S. de Melo, J.A.V. Del Carpio, W.B. Broering, Permanent deformation performance under moisture effect of an asphalt mixture modified by calcium carbonate nanoparticles, *Construct. Build. Mater.* 342 (2022) 128087.
- [69] Z.T. Al-Fayyadh, H.M. Al-Mosawe, The effect of rubber crumbs on marshall properties for warm mix asphalt, *J. Eng.* 29 (6) (2023) 46–59.
- [70] L. Huang, J. Geng, M. Chen, Y. Niu, W. Wang, Z. Gao, Investigation into the rheological properties and microstructure of silt/crumb rubber compound-modified asphalt, *Polymers* 15 (11) (2023) 2474.
- [71] G.J. Kashesh, H.H. Joni, A. Dulaimi, A.J. Kaishesh, Laboratory investigation on the performance of asphalt bitumen using recycled tyre rubber produced in Iraq, *Mater. Today: Proc.* 42 (2023) 2717–2724.
- [72] B. Yilmaz, A.M. Özdemiř, H.E. Gürbüz, Assessment of thermal properties of nanoclay-modified bitumen, *Arabian J. Sci. Eng.* 48 (4) (2023) 4595–4607.
- [73] T. Geckil, S. Issi, C.B. Ince, Evaluation of prina for use in asphalt modification, *Case Stud. Constr. Mater.* 17 (2022) e01623.
- [74] J. V. Staub de Melo Manfro, J.A. Villena Del Carpio, W.B. Broering, Permanent deformation performance under moisture effect of an asphalt mixture modified by calcium carbonate nanoparticles, *Construct. Build. Mater.* 342 (2022) 128087, <https://doi.org/10.1016/j.conbuildmat.2022.128087>, 2022/08/01/.
- [75] P.G.T.M. Filho, A.T. Rodrigues dos Santos, L.C.d.F.L. Lucena, V.F. de Sousa Neto, Rheological evaluation of asphalt binder 50/70 incorporated with titanium dioxide nanoparticles, *J. Mater. Civ. Eng.* 31 (10) (2019) 04019235.
- [76] A. Raufi, B. Şengöz, D. Kaya Özdemiř, Assessment of asphalt binders and hot mix asphalt modified with nanomaterials, *Period. Polytech. Civ. Eng.* 64 (1) (2020).

- [77] P. Caputo, M. Porto, R. Angelico, V. Loise, P. Calandra, C. Oliviero Rossi, Bitumen and asphalt concrete modified by nanometer-sized particles: basic concepts, the state of the art and future perspectives of the nanoscale approach, *Adv. Colloid Interface Sci.* 285 (2020) 102283, <https://doi.org/10.1016/j.cis.2020.102283>, 2020/11/01/.
- [78] H.H. Joni, H.H. Zghair, A.A. Mohammed, Rutting parameters of modified asphalt binder with micro and nano-size of metakaolin powder, *J. Eng. Sci. Technol.* 15 (5) (2020) 3465–3480.
- [79] Z. Zhao, et al., Recycling waste disposable medical masks in improving the performance of asphalt and asphalt mixtures, *Construct. Build. Mater.* 337 (2022) 127621.
- [80] X.H. Hao, Y.M. Wang, A.Q. Zhang, A study on improving the adhesiveness between granite and asphalt by nano-scaled calcium carbonate, *Key Eng. Mater.* 575 (2014) 54–57.
- [81] R.A. Al-Mansob, et al., The performance of Epoxidised Natural Rubber modified asphalt using nano-alumina as additive, *Construct. Build. Mater.* 155 (2017) 680–687, <https://doi.org/10.1016/j.conbuildmat.2017.08.106>, 2017/11/30/.
- [82] B. Golestani, F. Moghadas Nejad, S. Sadeghpour Galooyak, Performance evaluation of linear and nonlinear nanocomposite modified asphalts, *Construct. Build. Mater.* 35 (2012) 197–203, <https://doi.org/10.1016/j.conbuildmat.2012.03.010>, 2012/10/01/.
- [83] S.I.A. Ali, A. Ismail, M.R. Karim, N.I.M. Yusoff, R.A. Al-Mansob, E. Aburkaba, Performance evaluation of Al₂O₃ nanoparticle-modified asphalt binder, *Road Mater. Pavement Des.* 18 (6) (2017) 1251–1268.
- [84] A.A. Hussein, R.P. Jaya, N.A. Hassan, H. Yaacob, G.F. Huseien, M.H.W. Ibrahim, Performance of nanoceramic powder on the chemical and physical properties of bitumen, *Construct. Build. Mater.* 156 (2017) 496–505.
- [85] J. Wang, et al., Performance evaluation of aged asphalt rejuvenated with various bio-oils based on rheological property index, *J. Clean. Prod.* 385 (2023) 135593, <https://doi.org/10.1016/j.jclepro.2022.135593>, 2023/01/20/.
- [86] S.N.A. Jeffry, R. Putra Jaya, N. Abdul Hassan, H. Yaacob, M.Z.H. Mahmud, Z.H. Al-Saffar, The influence of nano-carbon from coconut shell ash as modifier on the properties of bitumen, *Road Mater. Pavement Des.* 23 (4) (2022) 770–786.
- [87] Z.H.H. Al-Saffar, Performance of Reclaimed Asphalt Pavement Rejuvenated With Maltene, PhD, Civil Engineering, UTM, 2021.
- [88] S. Ren, X. Liu, P. Lin, R. Jing, S. Erkens, Toward the long-term aging influence and novel reaction kinetics models of bitumen, *Int. J. Pavement Eng.* (2022) 1–16.
- [89] Z. Li, C. Fa, H. Zhao, Y. Zhang, H. Chen, H. Xie, Investigation on evolution of bitumen composition and micro-structure during aging, *Construct. Build. Mater.* 244 (2020) 118322.
- [90] X. Li, et al., Effect of graphene on modified asphalt microstructures based on atomic force microscopy, *Materials* 14 (13) (2021) 3677. <https://www.mdpi.com/1996-1944/14/13/3677>.
- [91] H.-R. Wang, et al., Properties and mechanism of phase-change bitumen with polyurethane shell microencapsulated as modifier, *Case Stud. Constr. Mater.* 19 (2023) e02249, <https://doi.org/10.1016/j.cscm.2023.e02249>, 2023/12/01/.
- [92] R. De Oliveira, D. Albuquerque, T. Cruz, F. Yamaji, F. Leite, Measurement of the nanoscale roughness by atomic force microscopy: basic principles and applications, in: *Atomic Force Microscopy-Imaging, Measuring and Manipulating Surfaces at the Atomic Scale*, 3, 2012.
- [93] S.A.P. Rosyidi, et al., Physical, chemical and thermal properties of palm oil boiler ash/rediset-modified asphalt binder, *Sustainability* 14 (2022) 3018, <https://doi.org/10.3390/su14053016>, 03/04.
- [94] N.M. Akhira, et al., Microstructural and thermal analysis of warm-modified bitumen with palm oil boiler ash, *J. Kejuruteraan* 35 (3) (2023) 675–681.
- [95] K.S.P. Karunadasa, C.H. Manoratne, H.M.T.G.A. Pitawala, R.M.G. Rajapakse, Thermal decomposition of calcium carbonate (calcite polymorph) as examined by in-situ high-temperature X-ray powder diffraction, *J. Phys. Chem. Solid.* 134 (2019) 21–28, <https://doi.org/10.1016/j.jpcs.2019.05.023>, 2019/11/01/.